Manuscript Number: **angeo-2019-79**

Article Title: **Global TEC prediction performance assessment of IRI-2016 model based on EOF decomposition**

Dear Editor,

We would like to thank Annales Geophysicae for giving us the opportunity to revise our manuscript. We thank the reviewers for their careful read and thoughtful comments on previous draft. We have carefully taken their comments into consideration in preparing our revision, and hope that the corrections will meet with approval. Revised portion are marked in blue in the marked-up manuscript. The following summarizes how we responded to reviewer comments.

Below is our response to their comments.

Thanks for all the help.

Best wishes.

Yours sincerely,
Dr. Shuhui LI
Corresponding Author

Revision — authors' response

Reviewer #1:

Review comments on manuscript "Global TEC prediction performance assessment of IRI-2016 model based on EOF decomposition" by Li et al., 2019; submitted to Annales Geophysicae

The manuscript compares total electron content from Global Ionospheric Maps products and International Reference Ionosphere during 2013. Empirical Orthogonal Functions are employed to detail the differences between the two datasets.

Seasonal average analysis was performed which showed that the IRI model reproduces the equatorial ionisation anomaly distinctively while GIM TEC does show enhancement of TEC over equatorial/low latitude regions, but does not necessarily show the different bands of enhancement at the EIA crests. While related studies exist, I think this work is relevant especially if it clearly shows by how much the IRI under-predicts GIM TEC (in terms of TECu) in different latitude regions. However this is not clearly shown in the current paper.

Answer: According to the reviewer's suggestion, we have added some analysis and discussion about the discrepancies between GIM-TEC and IRI-TEC at different latitudes as follows in the revised manuscript: Considering the different levels of ionospheric activities at different latitudes, mean and RMS values of the discrepancies between seasonal averages of GIM-TEC and IRI-TEC over different latitudinal regions in 2013 were calculated. Results are shown in Figure 2. From Figure 2, the mean and RMS values over the area near the equator generally exhibit peak values. GIM-TEC values over the equator and low latitudes are much larger than IRI-TEC values, especially over the ionospheric trough near the magnetic equator shown in Figure 1. The mean and RMS values over Southern Hemisphere during the December solstice are significantly large and also very large over Northern Hemisphere during the June solstice. Therefore, there are large discrepancies between GIM-TEC and IRI-TEC over the summer Hemisphere.

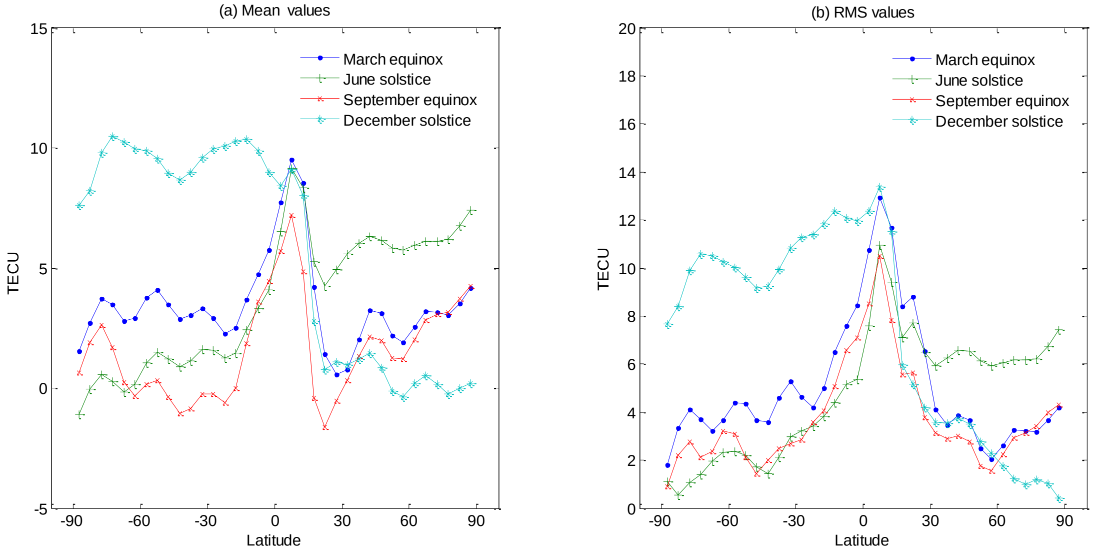

Figure 2. Mean and RMS values of the discrepancies between GIM-TEC and IRI-TEC at different latitudes during four seasons.

Additionally, as the authors know, the IRI model provides TEC up to an altitude of 2000 km while GIM TEC products are based on GNSS observations (at about 20000 km). Assuming that the IRI model was 'accurate' at its specified height, it would be missing some plasmaspheric contribution. The authors have missed to point out this important aspect early in the paper. I believe it is related to line 10, page 6, and Figure 1. Information about this is later presented on page 15, line 10.

Answer: According to the reviewer's instruction, we advanced the relevant paragraph as follows on page 15 to page 6 in the revised manuscript:

“The IRI-2016 model provides ionospheric parameters of up to 2000 km and will inaccurately predict the TEC up to GNSS satellites located at an altitude of approximately 20,000 km. The IRI-TEC may be smaller than GIM-TEC because of the missing plasmaspheric content.”

On page 15, we changed the statement as follows:

“Although the IRI-TEC will be smaller than the GIM-TEC because of the missing plasmaspheric content, A_{11} of IRI-TEC in Figure 10(b) shows a quite large underestimation compared with that of GIM-TEC.”

Below are comments which may assist in improving the paper.

Page 3, line 35: I thought that the GIM TEC products are provided at time resolution of 2 hours. Please cross-check that they are also available for 15 minutes.

Answer: According to the reviewer’s suggestion, we have checked the temporal resolution of IGS GIMs. In terms of temporal resolution, the GIM generated by each IAAC and IGS is different. Final GIMs produced by CODE, ESA, JPL and UPC are provided with a 2h temporal resolution, whereas the CODE-produced IONEX maps are in 1-hour temporal resolution. The temporal resolution of CASG GIMs is 0.5-hour.

In order to describe it more accurately, we changed the expression as follows in the revised manuscript:

“The GIM TEC used in this study is the official IGS combined final product provided by the Crustal Dynamic Data Information System (ftp://cddis.gsfc.nasa.gov). Final GIMs are regular products of the International GNSS Service (IGS) since 1998. These GIMs are provided in the ionosphere exchange format with a spatial resolution of 2.5°×5° in geographic latitude and longitude and a temporal resolution of 2 h.”

Page 4, line 5, please include original references for the hmF2 model options included within the IRI 2016 model. One is based on COSMIC observations (Shubin) and the other one on ionosonde measurements and spheric harmonic method (Altadil).

Answer: According to the reviewer's instruction, we have added original references for the hmF2 model options included within the IRI 2016 model in the revised manuscript as follows:

“The recent version of this model is IRI-2016 (Bilitza et al., 2016; Bilitza et al., 2017). After IRI-2012, IRI-2016 exhibits the latest improvement in the model by introducing two new F2 peak height hmF2 modeling options with their data sources from ionosonde measurements (Altadill et al., 2013) and COSMIC radio occultations (Shubin, 2015)."

Altadill, D., Magdaleno, S., Torta, J. M., Blanch, E.: Global empirical models of the density peak height and of the equivalent scale height for quiet conditions, Adv. Space Res., 52, 1756–1769, https://doi.org/10.1016/j.asr.2012.11.018, 2013.

Shubin, V. N.: Global median model of the F2-layer peak height based on ionospheric radio-occultation and ground-based Digisonde observations, Adv. Space Res., 56, 916–928, https://doi.org/10.1016/j.asr.2015.05.029, 2015.

Page 4, line 10: In the statement "The global TEC date calculated ...". The word 'date' should be data.

Answer: Yes, it is a mistake. We changed "date" to "**data**" in revised version. Thank you.

Page 5, line 5 is not clear. In the text "If the IRI TEC and GIM TEC are decomposed, then their EOF base functions and coefficients will exhibit poor comparability". Why would this be the case? And do you mean that this would be so, if they were decomposed separately? Assuming that they exhibit some similarities/differences, wouldn't such decomposition bring them out? May be not in magnitude of coefficients or base functions; but perhaps in the trend and identification of physical features?

Answer: This sentence is indeed unclear. As you understand, what we want to express is that if they are decomposed separately, it will be difficult to compare in magnitude. We changed the sentence to "If the IRI TEC and GIM TEC are decomposed separately, it is difficult to directly compare their EOF base functions and coefficients in magnitude." in revised version.

The spatial patterns and temporal variations of the global TEC data are separated by EOF decomposition and can be properly represented by the base functions and associated coefficients, respectively. For GIM-TEC data X_{GIM} , coefficients $A_{k,\ GIM}$ and EOF base functions $E_{k,GIM}$ will be obtained by using EOF decomposition method. For IRI-TEC data X_{IRI} , the coefficients $A_{k,IRI}$ and EOF base functions $E_{k,IRI}$ can be obtained:

$$X_{GIM} = \sum_{k=1}^{N} E_{k,GIM} \cdot A_{k,\ GIM}$$

$$X_{IRI} = \sum_{k=1}^{N} E_{k,IRI} \cdot A_{k,IRI}$$

EOF decomposition will extract main spatial patterns. The six main base functions E_k extracted by performing EOF decomposition on the global TEC from related reference (Talaat and Zhu, 2016) and our study both include the following: the variation with the geomagnetic latitude reflecting the daily averaged solar forcing, the diurnal and semidiurnal periodic changes with longitude due to local time, and the interhemispheric asymmetry caused by the annual variation of the inclination angle of the Earth's orbit.

The spatiotemporal features extracted from IRI-TEC and GIM-TEC data have good consistencies, they are shown in Figs (2) and (3) of this document. Therefore, if GIM-TEC and IRI-TEC are decomposed separately, the results will exhibit obvious similarities in trend and identification of physical features. However, it is not possible to make direct comparisons in magnitude, because $A_{k,\ GIM}$ and $A_{k,IRI}$ are different, $E_{k,GIM}$ and $E_{k,IRI}$ are also different.

So we combined the data to form a whole data set for EOF decomposition and compared the two data sets.

$$\begin{bmatrix} X_{GIM} \\ X_{IRI} \end{bmatrix} = \sum_{k=1}^{N} \begin{bmatrix} E_{k,GIM} \\ E_{k,IRI} \end{bmatrix} \cdot A_k$$

Then, the GIM-TEC and IRI-TEC can be written and reconstruct as follows.

$$X_{GIM} = \sum_{k=1}^{N} E_{k,GIM} \cdot A_k$$

$$X_{IRI} = \sum_{k=1}^{N} E_{k,IRI} \cdot A_k$$

The same coefficients of the EOF base function A_k can be obtained, then $E_{k,GIM}$ and $E_{k,IRI}$ were compared to analyze the difference between GIM-TEC and IRI-TEC. We think the conclusions obtained by the method of this paper are clearer.

Following on the previous comment, do you mean that IRI TEC and GIM TEC are combined to form one data file which is later used for decomposition?

Answer: Yes, IRI TEC and GIM TEC are combined to form one data file which is later used for decomposition.

The two sets of data are arranged in rows or columns as needed.

In our study, We analyzed the global TEC over a 1 year time period (2013) with a 2 h temporal resolution and 37×36=1332 spatial grids, the total epoch number is 12×365=4380. Before EOF analysis, GIM TEC data X_{GIM} should be arranged as follows:

$$\underset{1332\times4380}{X_{GIM}} = \begin{bmatrix} \mathrm{TEC}^{\mathrm{GIM}}_{\mathrm{grid1,epoch1}} & \mathrm{TEC}^{\mathrm{GIM}}_{\mathrm{grid2,epoch2}} & \cdots & \mathrm{TEC}^{\mathrm{GIM}}_{\mathrm{grid1,epoch4380}} \\ \mathrm{TEC}^{\mathrm{GIM}}_{\mathrm{grid2,epoch1}} & \mathrm{TEC}^{\mathrm{GIM}}_{\mathrm{grid2,epoch2}} & \cdots & \mathrm{TEC}^{\mathrm{GIM}}_{\mathrm{grid2,epoch4380}} \\ \vdots & \vdots & \ddots & \vdots \\ \mathrm{TEC}^{\mathrm{GIM}}_{\mathrm{grid1332,epoch1}} & \mathrm{TEC}^{\mathrm{GIM}}_{\mathrm{grid1332,epoch2}} & \cdots & \mathrm{TEC}^{\mathrm{GIM}}_{\mathrm{grid1332,epoch4380}} \end{bmatrix}$$

Coefficients $A_{k,\ GIM}$ and EOF base functions $E_{k,GIM}$ will be obtained by using EOF decomposition method:

$$X_{GIM} = \sum_{k=1}^{N} E_{k,GIM} \cdot A_{k,\ GIM}$$

The same coefficients of the EOF base function, that is, the same time-varying features, can be obtained by arranging IRI-TEC and GIM-TEC according to the same number of columns. That is：

$$\underset{2664\times4380}{\begin{bmatrix} X_{GIM} \\ X_{IRI} \end{bmatrix}} = \begin{bmatrix} \mathrm{TEC}^{\mathrm{GIM}}_{\mathrm{grid1,epoch1}} & \mathrm{TEC}^{\mathrm{GIM}}_{\mathrm{grid2,epoch2}} & \cdots & \mathrm{TEC}^{\mathrm{GIM}}_{\mathrm{grid1,epoch4380}} \\ \mathrm{TEC}^{\mathrm{GIM}}_{\mathrm{grid2,epoch1}} & \mathrm{TEC}^{\mathrm{GIM}}_{\mathrm{grid2,epoch2}} & \cdots & \mathrm{TEC}^{\mathrm{GIM}}_{\mathrm{grid2,epoch4380}} \\ \vdots & \vdots & \ddots & \vdots \\ \mathrm{TEC}^{\mathrm{GIM}}_{\mathrm{grid1332,epoch1}} & \mathrm{TEC}^{\mathrm{GIM}}_{\mathrm{grid1332,epoch2}} & \cdots & \mathrm{TEC}^{\mathrm{GIM}}_{\mathrm{grid1332,epoch4380}} \\ \mathrm{TEC}^{\mathrm{IRI}}_{\mathrm{grid1,epoch1}} & \mathrm{TEC}^{\mathrm{IRI}}_{\mathrm{grid1,epoch2}} & \cdots & \mathrm{TEC}^{\mathrm{IRI}}_{\mathrm{grid1,epoch4380}} \\ \mathrm{TEC}^{\mathrm{IRI}}_{\mathrm{grid2,epoch1}} & \mathrm{TEC}^{\mathrm{IRI}}_{\mathrm{grid2,epoch2}} & \cdots & \mathrm{TEC}^{\mathrm{IRI}}_{\mathrm{grid2,epoch4380}} \\ \vdots & \vdots & \ddots & \vdots \\ \mathrm{TEC}^{\mathrm{IRI}}_{\mathrm{grid1332,epoch1}} & \mathrm{TEC}^{\mathrm{IRI}}_{\mathrm{grid1332,epoch2}} & \cdots & \mathrm{TEC}^{\mathrm{IRI}}_{\mathrm{grid1332,epoch4380}} \end{bmatrix}$$

Then, we will get EOF decomposition result:

$$\begin{bmatrix} X_{GIM} \\ X_{IRI} \end{bmatrix} = \sum_{k=1}^{N} \begin{bmatrix} E_{k,GIM} \\ E_{k,IRI} \end{bmatrix} \cdot A_k$$

Then, the GIM-TEC and IRI-TEC can be written as follows.

$$X_{GIM} = \sum_{k=1}^{N} E_{k,GIM} \cdot A_k$$

$$X_{IRI} = \sum_{k=1}^{N} E_{k,IRI} \cdot A_k$$

It seems like that we extract common temporal variation factors A_k, and we can therefore directly compare the spatial characteristics $E_{k,GIM}$ and $E_{k,IRI}$.

Page 7, Table 1, indicate the units of some parameters; maximum, minimum and mean bias; e.g mean bias (TECU).

Answer: According to the reviewer’s suggestion, we added the units of Maximum bias, Minimum bias and Mean bias in Table 1 in the revised manuscript.

Page 6, just after line 15: Bias values are computed using IRI TEC and GIM TEC? It is not clear how daily RMS values in 2013 displayed in Figure 2 are computed. Are they just average of the bias values calculated using IRI TEC and GIM TEC?

Answer: The sentence about how to calculate RMS in line 16, Page 6 is not clear. We changed it as follows in the revised manuscript:

"The gridded values of the global IRI-TEC and GIM-TEC at different UTs for each day of the year 2013 were used to calculate the daily RMS."

The expression of equation (10) in our manuscript is also not clear, so we changed " $RMS = \left[\sum_i^n (Y_i - Y_i')^2 / n \right]^{1/2}$ " to " $RMS = \sqrt{\frac{1}{n}\sum_i^n (Y_i - Y_i')^2}$ " in the revised manuscript.

During a day, the global TEC data has 1322 grid points and 12 epochs. Therefore, both the GIM-TEC data and IRI-TEC data for one day have 1332*12=15984 values.

Daily RMS value in 2013 displayed in Figure 2 is computed by using equation (10):

$$RMS = \sqrt{\frac{1}{n}\sum_i^n (Y_i - Y_i')^2}$$

Where, n=15984, Y_i and Y_i' are data for GIM-TEC and IRI-TEC respectively.

Page 5, equation 10: Shouldn't RMS be RMSE? This seems to be what is plotted in Figure 2(a). RMSE values of IRI 2016, how are they computed?

Answer: Yes, here is a mistake. RMS and RMSE should be unified. We examined the entire manuscript and used "RMS" in all equations and figures in the revised manuscript.

Under subsection 3.2: the authors state "We combined the IRI TEC and GIM TEC data ...". If these datasets are combined, how do you obtain Figure 4?

Answer: We combined the data as follows:

$$\begin{bmatrix} X_{GIM} \\ X_{IRI} \end{bmatrix}_{2664\times 4380} = \begin{bmatrix} \mathrm{TEC}^{\mathrm{GIM}}_{\mathrm{grid1,epoch1}} & \mathrm{TEC}^{\mathrm{GIM}}_{\mathrm{grid2,epoch2}} & \cdots & \mathrm{TEC}^{\mathrm{GIM}}_{\mathrm{grid1,epoch4380}} \\ \mathrm{TEC}^{\mathrm{GIM}}_{\mathrm{grid2,epoch1}} & \mathrm{TEC}^{\mathrm{GIM}}_{\mathrm{grid2,epoch2}} & \cdots & \mathrm{TEC}^{\mathrm{GIM}}_{\mathrm{grid2,epoch4380}} \\ \vdots & \vdots & \ddots & \vdots \\ \mathrm{TEC}^{\mathrm{GIM}}_{\mathrm{grid1332,epoch1}} & \mathrm{TEC}^{\mathrm{GIM}}_{\mathrm{grid1332,epoch2}} & \cdots & \mathrm{TEC}^{\mathrm{GIM}}_{\mathrm{grid1332,epoch4380}} \\ \mathrm{TEC}^{\mathrm{IRI}}_{\mathrm{grid1,epoch1}} & \mathrm{TEC}^{\mathrm{IRI}}_{\mathrm{grid1,epoch2}} & \cdots & \mathrm{TEC}^{\mathrm{IRI}}_{\mathrm{grid1,epoch4380}} \\ \mathrm{TEC}^{\mathrm{IRI}}_{\mathrm{grid2,epoch1}} & \mathrm{TEC}^{\mathrm{IRI}}_{\mathrm{grid2,epoch2}} & \cdots & \mathrm{TEC}^{\mathrm{IRI}}_{\mathrm{grid2,epoch4380}} \\ \vdots & \vdots & \ddots & \vdots \\ \mathrm{TEC}^{\mathrm{IRI}}_{\mathrm{grid1332,epoch1}} & \mathrm{TEC}^{\mathrm{IRI}}_{\mathrm{grid1332,epoch2}} & \cdots & \mathrm{TEC}^{\mathrm{IRI}}_{\mathrm{grid1332,epoch4380}} \end{bmatrix}$$

After performing EOF decomposition, we will get:

$$\begin{bmatrix} X_{GIM} \\ X_{IRI} \end{bmatrix}_{2664\times 4380} = \sum_{k=1}^{N} \underset{2664\times 1}{E_k} \cdot \underset{4380\times 1}{A_k} = \sum_{k=1}^{N} \underset{2664\times 1}{\begin{bmatrix} E_{k,GIM} \\ E_{k,IRI} \end{bmatrix}} \cdot \underset{4380\times 1}{A_k} = \begin{bmatrix} \sum_{k=1}^{N} \underset{1332\times 1}{E_{k,GIM}} \cdot \underset{4380\times 1}{A_k} \\ \sum_{k=1}^{N} \underset{1332\times 1}{E_{k,IRI}} \cdot \underset{4380\times 1}{A_k} \end{bmatrix}$$

$$\underset{1332\times 4380}{X_{GIM}} = \sum_{k=1}^{N} \underset{1332\times 1}{E_{k,GIM}} \cdot \underset{4380\times 1}{A_k}$$

$$\underset{1332\times 4380}{X_{IRI}} = \sum_{k=1}^{N} \underset{1332\times 1}{E_{k,IRI}} \cdot \underset{4380\times 1}{A_k}$$

That is to say, the two sets of data are arranged together, and after the common coefficients are extracted, the base functions $\underset{2664\times 1}{E_k}$ are separated to $\begin{bmatrix} E_{k,GIM} \\ E_{k,IRI} \end{bmatrix}$. So we can get two sets of base functions: $\underset{1332\times 1}{E_{k,GIM}}$ and $\underset{1332\times 1}{E_{k,IRI}}$, which are shown in Figure 4.

In order to make the expression clearer, we revised equations (6) and (7) in page 5:

"$$\begin{bmatrix} X_{GIM} \\ X_{IRI} \end{bmatrix} = \sum_{k=1}^{N} \begin{bmatrix} E_{k,GIM} \\ E_{k,IRI} \end{bmatrix} \cdot A_k = \begin{bmatrix} \sum_{k=1}^{N} E_{k,GIM} \cdot A_k \\ \sum_{k=1}^{N} E_{k,IRI} \cdot A_k \end{bmatrix} \quad (6)$$

$$[X_{GIM} \quad X_{IRI}] = \sum_{k=1}^{N} E_k \cdot \begin{bmatrix} A_{k,GIM} & A_{k,IRI} \end{bmatrix} = \begin{bmatrix} \sum_{k=1}^{N} E_k \cdot A_{k,GIM} & \sum_{k=1}^{N} E_k \cdot A_{k,IRI} \end{bmatrix} \quad (7)$$"

In Figure 3, is global data for 2013 used? How do you account for latitudinal differences? Does this figure reflect only seasonal changes as indicated in the last statement on page 7?

Answer: Yes, global data for 2013 is used in Figure 3.

The EOF decomposition was conducted on GIM-TEC and IRI-TEC as follow,

$$\underset{2664\times 4380}{\begin{bmatrix} X_{GIM} \\ X_{IRI} \end{bmatrix}} = \sum_{k=1}^{N} \underset{2664\times 1}{\begin{bmatrix} E_{k,GIM} \\ E_{k,IRI} \end{bmatrix}} \cdot \underset{4380\times 1}{A_k} = \begin{bmatrix} \sum_{k=1}^{N} \underset{1332\times 1}{E_{k,GIM}} \cdot \underset{4380\times 1}{A_k} \\ \sum_{k=1}^{N} \underset{1332\times 1}{E_{k,IRI}} \cdot \underset{4380\times 1}{A_k} \end{bmatrix}$$

The spatial patterns and temporal variations of the TEC are separated by EOF decomposition and can be properly represented by the base functions and associated coefficients, respectively. $\underset{2664\times 1}{\begin{bmatrix} E_{k,GIM} \\ E_{k,IRI} \end{bmatrix}}$ represent the TEC's spatial distribution modes, and they are base functions. Six main base functions are shown in Figure 4. And $\underset{4380\times 1}{A_k}$ represents the magnitude of the influence of the k th base function component at different epoch. Six coefficients of main base function $\underset{4380\times 1}{A_k}$ are shown in Figure 3.

Therefore, Figure 3 reflects only seasonal changes, while Figure 4 represents the spatial distribution characteristics.

Equation 7 and Figure 7: I am not sure of the physical significance and justification of combining IRI TEC and GIM TEC. Afterall, they have different inherent errors. What can be derived from this combination taken at same grid points can as well be determined from one dataset either GIM TEC or IRI TEC. Otherwise combining these datasets removes the differences/similarities that the authors would want to study? Provide a scientific justification for combining both datasets and what additional features or interpretations are obtained. I don't think that the text in line 15, page 15 is sufficient to justify this inclusion. This has already been discussed.

Answer: After performing EOF decomposition on GIM-TEC and IRI-TEC by using equation (7), we will get base functions E_k and coefficients A_k.

$$[X_{GIM} \quad X_{IRI}] = \sum_{k=1}^{N} E_k \cdot \begin{bmatrix} A_{k,GIM} & A_{k,IRI} \end{bmatrix} = \begin{bmatrix} \sum_{k=1}^{N} A_{k,GIM} \cdot E_k & \sum_{k=1}^{N} A_{k,IRI} \cdot E_k \end{bmatrix} \quad (7)$$

However, the original TEC data can be reconstructed by using E_k and A_k as follow:

$$X_{GIM} = \sum_{k=1}^{N} A_{k,GIM} \cdot E_k$$

$$X_{IRI} = \sum_{k=1}^{N} A_{k,IRI} \cdot E_k$$

In other words, the EOF decomposition process of equation (7) is reversible. Therefore, decomposition after combining the two sets of data does not lead to errors.

We showed the six main base functions E_k extracted from combined data of IRI TEC and GIM TEC by using Equation (7) in Figure (1). And we also performed EOF decomposition on GIM-TEC and IRI-TEC separately by using Eqs (a) and (b), the base function $E_{k,GIM}$ and $E_{k,IRI}$ are shown in Figs (2) and (3).

$$X_{GIM} = \sum_{k=1}^{N} E_{k,GIM} \cdot A_{k,\ GIM} \quad (a)$$

$$X_{IRI} = \sum_{k=1}^{N} E_{k,IRI} \cdot A_{k,IRI} \qquad \text{(b)}$$

Although E_k in Figure (1) extracted from combined data is not as same as $E_{k,GIM}$ or $E_{k,IRI}$ in Figs (2) and (3), they do reflect consistent spatial distribution characteristics of global TEC.

Only if common base functions E_k of Equation (7) are used, we can compare $A_{k,GIM}$ and $A_{k,IRI}$ directly. The results will show the difference of the intensity of each base function between GIM-TEC and IRI-TEC.

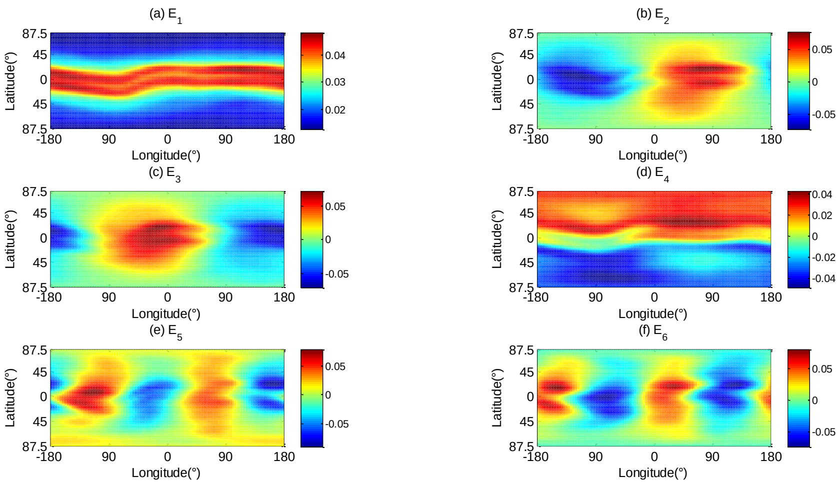

Figure (1). Base function E_k extracted from combined data of GIM-TEC and IRI-TEC

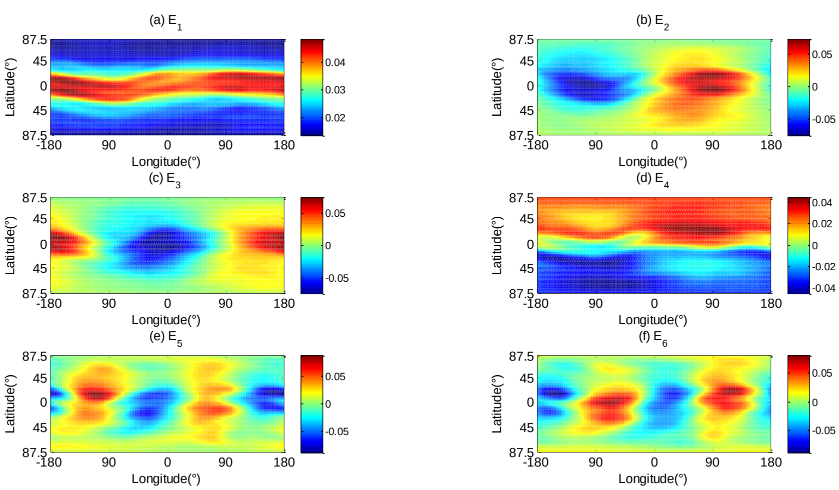

Figure (2). Base function $E_{k,GIM}$ extracted from GIM-TEC

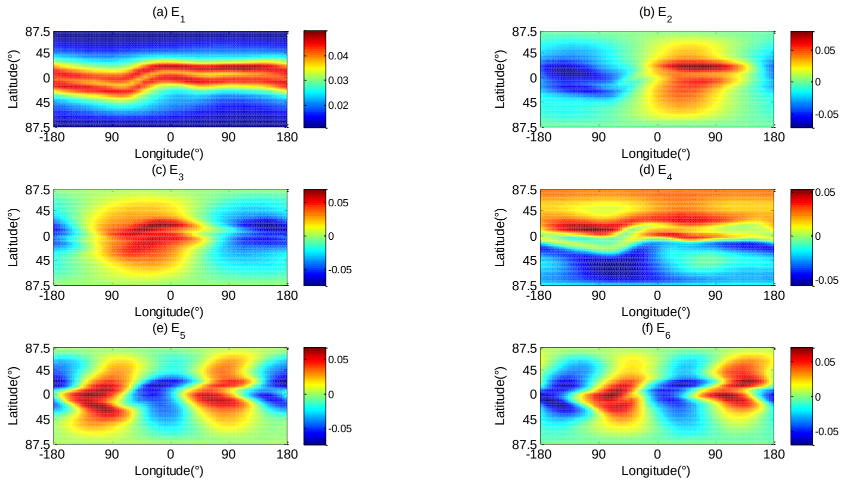

Figure (3). Base function $E_{k,IRI}$ extracted from IRI-TEC

Unless I am not understanding equation 7, how do you separately derive A1-A6 for GIM TEC and IRI TEC that you have plotted in Figure 8? Once again, is this necessary? What additional information do we get in Figure 8?

Answer: Maybe the equation (7) is not so clear, we have changed it as follows:

"$$[X_{GIM} \quad X_{IRI}] = \sum_{k=1}^{N} E_k \cdot [A_{k,GIM} \quad A_{k,IRI}] = \left[\sum_{k=1}^{N} E_k \cdot A_{k,GIM} \quad \sum_{k=1}^{N} E_k \cdot A_{k,IRI}\right] \qquad (7)$$"

Then, GIM-TEC and IRI-TEC can be written:

$$X_{GIM} = \sum_{k=1}^{N} E_k \cdot A_{k,GIM}$$

$$X_{IRI} = \sum_{k=1}^{N} E_k \cdot A_{k,IRI}$$

Therefore, we can get $A_{k,GIM}$ for GIM-TEC and $A_{k,IRI}$ for IRI-TEC, which are shown in Figure 8. From Figure 8, we can see that the variation of A_1 is strongly correlated with solar activity. A_2 and A_3 have a diurnal variation with UT, and also have a semiannual cycle. A_4 has a distinct annual cycle, and A_5 and A_6 exhibit a semidiurnal cycle and a semiannual cycle. GIM-TEC and IRI-TEC have good consistencies in the above period terms, but the comparison of specific difference in each periodic variation is difficult.

So, we conducted EOF decomposition on $A_1 - A_6$ according to the equation (13) to divide diurnal variation with UT and seasonal variation characteristics of $A_{k,GIM}$ and $A_{k,IRI}$. The results are shown in Figure 9. Therefore, the article continued to discuss the differences between t $A_{k,GIM}$ and $A_{k,IRI}$ based on Figure 9.

We have added some discussion about Figure 8 in the revised manuscript as follows:

"The time-varying characteristics of the coefficients in Figure 8 are very consistent with the results shown in Figure 3. From Figs. 8(a) and (b), the variations of A_1 are mainly related to solar activity, and solar activity is the primary determinant of the first base function E_1 in Figure 7(a), which describes the overall average of global TEC. From Figs. 8(c)–(f), the EOF coefficients A_2 and A_3 of GIM-TEC and IRI-TEC all obviously exhibit a diurnal period and a semiannual period. They reflect the diurnal variation of solar radiation change with longitude due to the LT. A_4 in Figs. 8(g) and (h) indicate a strong annual cycle variation of the interhemispheric asymmetry of the TEC. A_5 and A_6 show a semiannual period of the base functions E_5 and E_6, which represent a longitudinal variation that changes with LT. The EOF coefficients of GIM-TEC and IRI-TEC have consistent annual, semiannual, diurnal, and semidiurnal variations. Therefore, Figure 8 manifests that GIM-TEC and IRI-TEC have highly consistent temporal variation characteristics based on the same spatial distribution modes E_k according to equation (7)."

Special thanks to you for your good comments and suggestions.

Reviewer #2:

The paper is very interesting and it is a contribution to IRI-2016 performance, which is always welcome. It uses a statistical technique (EOF) which sometimes is a bit confusing to understand. At least it is my opinion. But overall the paper presents the main differences which are well explained. I have only some additional comments to those made by Reviewer 1.

Main comments:

In page 5 you mention "Figure 2 demonstrates that the daily predicted RMS of IRI-2016 is in good agreement with the daily solar F10.7 index." If the bias is the deviation from GIM, it is not trivial that it should depend on solar activity level. Why is this?

Answer: Fig.2 demonstrates the RMS of bias value of the IRI-TEC and GIM-TEC. Relate research showed that the accuracies of GIM are about 4.0-4.5TECu. Therefore, GIM-TEC data were used as reference values in our study. The ionosphere is ionized by solar radiation, and the correlation coefficient between the global average TEC parameter calculated by GIM and the F10.7 index can reach approximately 0.9. From Fig.2, the ionospheric TEC prediction error of the IRI-2016 model presents a strong correlation with solar activity. We think there are two reasons. On the one hand, when the solar activity is strong, the TEC changes will be more intense. On the other hand, the IRI model does not fully describe the changing characteristics of the ionosphere with solar activity, and this can be verified in the comparison of the later part of the article. In Fig.9, we compared the time variation of IRI-TEC and GIM-TEC based on the same spatial variation component. The solar activity F10.7 index is also given on the figure. The diurnal and semi-diurnal changes of GIM-TEC vary with the F10.7 index, but IRI-TEC values do not reflect this variation characteristics (Figs 9(d), (f), (j), and (l)). The variation of the IRI-TEC is closer to the smoothing effect of the GIM-TEC time variation.

Which is the data used for Figure 3 ? IRI or GIMS ? I do not understand what this Figure shows.

Answer:

The spatial patterns and temporal variations of the global TEC data are separated by EOF decomposition and can be properly represented by the base functions E_k and associated coefficients A_k, respectively. We combined the data to form a whole data set for EOF decomposition and compared the two data sets according eq.(6).

$$\begin{bmatrix} X_{GIM} \\ X_{IRI} \end{bmatrix} = \sum_{k=1}^{N} \begin{bmatrix} E_{k,GIM} \\ E_{k,IRI} \end{bmatrix} \cdot A_k \qquad (6)$$

Then, the GIM-TEC and IRI-TEC can be written and reconstruct as follows.

$$X_{GIM} = \sum_{k=1}^{N} E_{k,GIM} \cdot A_k$$

$$X_{IRI} = \sum_{k=1}^{N} E_{k,IRI} \cdot A_k$$

Therefore, the same coefficients of the EOF base function A_k can be obtained, and were shown in Fig. 3. The spatial patterns of GIM-TEC and IRI-TEC $E_{k,GIM}$ and $E_{k,IRI}$ are shown in Fig.4.

This analysis method allows us to clearly see the difference in the spatial variation patterns of the two sets of data.

Minor correction: At the end of page 3: "University Time (UT)" should be "Universal Time (UT)"

Answer: Yes, it is a mistake. We changed " University Time (UT)" to " Universal Time (UT)" in revised version. Thank you.

Special thanks to you for your good comments and suggestions.

List of changes
Revised portion are marked in blue in the marked-up manuscript.

1. **Page 3, Section 2.1**

We changed the expression about GIM TEC as follows:
"The GIM TEC used in this study is the official IGS combined final product provided by the Crustal Dynamic Data Information System (ftp://cddis.gsfc.nasa.gov). Final GIMs are regular products of the International GNSS Service (IGS) since 1998. These GIMs are provided in the ionosphere exchange format with a spatial resolution of 2.5°×5° in geographic latitude and longitude and a temporal resolution of 2 h."

2. **Page 4, Section 2.2**

We have added original references for the hmF2 model options included within the IRI 2016 model in the revised manuscript as follows:
"The recent version of this model is IRI-2016 (Bilitza et al., 2016; Bilitza et al., 2017). After IRI-2012, IRI-2016 exhibits the latest improvement in the model by introducing two new F2 peak height hmF2 modeling options with their data sources from ionosonde measurements (Altadill et al., 2013) and COSMIC radio occultations (Shubin, 2015)."

3. **Page 4, Section 2.2**

We changed "date" to "**data**" in revised version.

4. **Page 4, Section 2.3**

We changed " University Time (UT)" to " **Universal Time (UT)**" in revised version.

5. **Page 5, Section 2.3**

We changed the sentence "If IRI-TEC and GIM-TEC data are decomposed, then their EOF base functions and coefficients will exhibit poor comparability." to:
"If the IRI TEC and GIM TEC are decomposed separately, it is difficult to directly compare their EOF base functions and coefficients in magnitude."

6. **Page 5, Section 2.3**

We have changed Equation (6) from $\begin{bmatrix} X_{GIM} \\ X_{IRI} \end{bmatrix} = \sum_{k=1}^{N} A_k \cdot \begin{bmatrix} E_{k,GIM} \\ E_{k,IRI} \end{bmatrix}$ to:

$$\begin{bmatrix} X_{GIM} \\ X_{IRI} \end{bmatrix} = \sum_{k=1}^{N} \begin{bmatrix} E_{k,GIM} \\ E_{k,IRI} \end{bmatrix} \cdot A_k = \begin{bmatrix} \sum_{k=1}^{N} E_{k,GIM} \cdot A_k \\ \sum_{k=1}^{N} E_{k,IRI} \cdot A_k \end{bmatrix}.$$

7. **Page 5, Section 2.3**

We have changed Equation (7) from $[X_{GIM} \quad X_{IRI}] = \sum_{k=1}^{N} \begin{bmatrix} A_{k,GIM} & A_{k,IRI} \end{bmatrix} \cdot E_k$ to:

$$X_{GIM} \quad X_{IRI}] = \sum_{k=1}^{N} E_k \cdot \begin{bmatrix} A_{k,GIM} & A_{k,IRI} \end{bmatrix} = \begin{bmatrix} \sum_{k=1}^{N} E_k \cdot A_{k,GIM} & \sum_{k=1}^{N} E_k \cdot A_{k,IRI} \end{bmatrix}.$$

8. **Page 5, Section 2.4**

We have changed Equation (10) from $RMS = \left[\sum_{i}^{n} (Y_i - Y_i')^2 / n \right]^{1/2}$ to:

$$RMS = \sqrt{\frac{1}{n} \sum_{i}^{n} (Y_i - Y_i')^2} \ .$$

9. **Page 6, Section 3.1**

We advanced the relevant paragraph as follows on page 15 to page 6 in the revised manuscript:
"The IRI-2016 model provides ionospheric parameters of up to 2000 km and will inaccurately predict the TEC up to GNSS satellites located at an altitude of approximately 20,000 km. The IRI-TEC may be smaller than GIM-TEC because of the missing plasmaspheric content."

10. **Page 6. Section 3.1**

We have added some analysis and discussion about the discrepancies between GIM-TEC and IRI-TEC at different latitudes as follows in the revised manuscript:

Considering the different levels of ionospheric activities at different latitudes, mean and RMS values of the discrepancies between seasonal averages of GIM-TEC and IRI-TEC over different latitudinal regions in 2013 were calculated. Results are shown in Figure 2. From Figure 2, the mean and RMS values over the area near the equator generally exhibit peak values. GIM-TEC values over the equator and low latitudes are much larger than IRI-TEC values, especially over the ionospheric trough near the magnetic equator shown in Figure 1. The mean and RMS values over Southern Hemisphere during the December solstice are significantly large, and they are also very large over Northern Hemisphere during the June solstice. Therefore, there are large discrepancies between GIM-TEC and IRI-TEC over the summer Hemisphere.

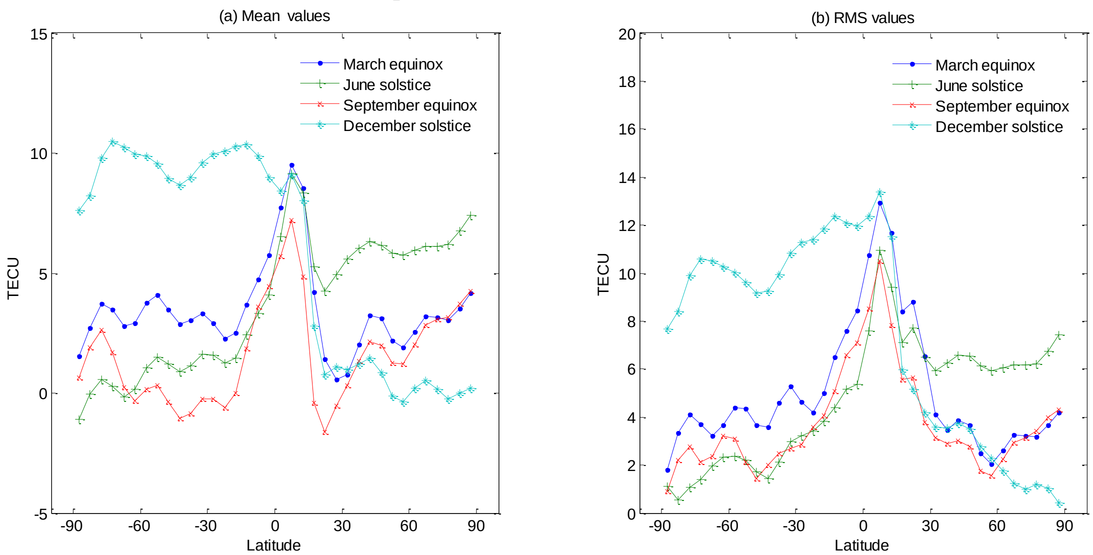

Figure 2. Mean and RMS values of the discrepancies between GIM-TEC and IRI-TEC at different latitudes during four seasons.

Due to the addition of a figure, the numbering of all subsequent pictures has changed.

11. Page 7, Section 3.1

We changed the sentence "The bias values between the IRI-TEC and GIM-TEC of all global grid points at different UTs were used to calculate the daily RMS in 2013." to:

"The gridded values of the global IRI-TEC and GIM-TEC at different UTs for each day of the year 2013 were used to calculate the daily RMS."

12. Page 7, Section 3.1

We changed "RMSE" to "RMS".

13. Page 8, Section 3.1

We added the unit "(TECU)" in Table 1.

14. Page 9, Section 3.2

We have modified the labels for the Y axe in Figure 5 (original Figure 4).

15. Page 11, Section 3.2

We added a "%" in Table 2.

16. Page 11, Section 3.2

We have modified the labels for the Y axe in Figure 6 (original Figure 5).

17. Page 12, Section 3.3

We have modified the labels for the Y axe in Figure 7 (original Figure 6).

18. Page 12, Section 3.3

We have changed the sentence "The figure manifests that the two data sets are highly consistent with the time variation of DOY and UT based on the same spatial distribution characteristics. The two sets of EOF coefficients have consistent annual, semiannual, diurnal, and semidiurnal changes." to:

The time-varying characteristics of the coefficients in Figure 9 are very consistent with the results shown in Figure 4. From Figs. 9(a) and (b), the variations of A_1 are mainly related to solar activity, and solar activity is the primary determinant of the first base function E_1 in Figure 8(a), which describes the overall average of global TEC. From Figs. 9(c)–(f), the EOF coefficients A_2 and A_3 of GIM-TEC and IRI-TEC all obviously exhibit a diurnal period and a semiannual period. They reflect the diurnal variation of solar radiation change with longitude due to the LT. A_4 in Figs. 9(g) and (h) indicate a strong annual cycle variation of the interhemispheric asymmetry of the TEC. A_5 and A_6 show a semiannual period of the base functions E_5 and E_6, which represent a longitudinal variation that changes with LT. The EOF coefficients of GIM-TEC and IRI-TEC have consistent annual, semiannual, diurnal, and semidiurnal variations. Therefore, Figure 9 manifests that GIM-TEC and IRI-TEC have highly consistent temporal variation characteristics based on the same spatial distribution modes E_k according to equation (7).

19. Page 13,Section 3.3

We added a "%" in Table 3.

20. Page 16, Section 3.3

We changed the sentences "The IRI-2016 model provides ionospheric parameters of up to 2000 km and will inaccurately predict the TEC up to GNSS satellites located at an altitude of approximately 20,000 km. The IRI-TEC may be smaller than GIM-TEC because of the missing plasmaspheric content.

Despite this situation, A_{11} of IRI-TEC in Figure 9(b) shows a larger underestimation compared with GIM-TEC." to:

"Although the IRI-TEC will be smaller than the GIM-TEC because of the missing plasmaspheric content, A_{11} of IRI-TEC in Figure 10(b) shows a quite large underestimation compared with that of GIM-TEC."

21. Page 16 and 17, References

We added the two references in the references list:

Altadill, D., Magdaleno, S., Torta, J. M., Blanch, E.: Global empirical models of the density peak height and of the equivalent scale height for quiet conditions, Adv. Space Res., 52, 1756–1769, https://doi.org/10.1016/j.asr.2012.11.018, 2013.

Shubin, V. N.: Global median model of the F2-layer peak height based on ionospheric radio-occultation and ground-based Digisonde observations, Adv. Space Res., 56, 916–928, https://doi.org/10.1016/j.asr.2015.05.029, 2015.

Global TEC prediction performance assessment of IRI-2016 model based on EOF decomposition

Shuhui Li[1,2], Jiajia Xu[1], Houxiang Zhou[1], Jinglei Zhang[1], Zeyuan Xu[1], Mingqiang Xie[1]

[1] School of Land Science and Technology, China University of Geosciences (Beijing), Beijing 100083, China
[2] Shanxi Key Laboratory of Resources, Environment and Disaster Monitoring, Jinzhong 221116, China

Correspondence to: Shuhui Li (li.shuhui@163.com)

Global TEC prediction performance assessment of IRI-2016 model based on EOF decomposition

Shuhui Li[1,2], Jiajia Xu[1], Houxiang Zhou[1], Jinglei Zhang[1], Zeyuan Xu[1], Mingqiang Xie[1]

[1] School of Land Science and Technology, China University of Geosciences (Beijing), Beijing 100083, China
[2] Shanxi Key Laboratory of Resources, Environment and Disaster Monitoring, Jinzhong 221116, China

Correspondence to: Shuhui Li (li.shuhui@163.com)

Abstract: In this study, the empirical orthogonal function (EOF) decomposition technique was utilized to analyze the similarities and differences of the spatiotemporal characteristics between the total electron content (TEC) of the International GNSS Service global ionospheric map (GIM) and that derived from the International Reference Ionosphere 2016 (IRI-2016) model in 2013. Results showed that the main spatial patterns and time-varying features of the data set have good consistency. The following four main spatiotemporal variation features can be extracted from both data sets through EOF decomposition: the variation with the geomagnetic latitude reflecting the daily averaged solar forcing, the diurnal and semidiurnal periodic changes with longitude due to local time, and the interhemispheric asymmetry caused by the annual variation of the inclination angle of the Earth's orbit. The differences between the spatial patterns represented by the EOF base functions of IRI-2016 and GIM TECs were analyzed by extracting the same time-varying coefficients. The deviations of the interhemispheric asymmetry component between the two data sets showed roughly equal values throughout the Southern or Northern Hemisphere, whereas those of the other spatial modes were mainly concentrated on the equatorial region. The differences of the time-varying characteristics between the IRI-2016 and GIM TECs were also compared by extracting the same EOF base functions. Although the EOF coefficients of the two data sets presented consistent seasonal variations, the magnitude of IRI-2016 TEC changes over time was less than that of GIM TEC. The diurnal variation of the daily averaged solar forcing component and the annual variation of the interhemispheric asymmetry component exhibited relatively large deviations between the two data sets. Considering the variance contribution of the different EOF components and their average relative deviations, both analyses showed that the daily averaged solar forcing and interhemispheric asymmetry components were the main factors for the deviation between the IRI-2016 and GIM TECs.

1 Introduction

The ionosphere is a shell of electrons and electrically charged atoms and molecules that surrounds the Earth and stretches from a height of approximately 60 km to more than 1000 km. The variations in the ionosphere should be accurately measured, modeled, or estimated because the ionosphere critically affects high-frequency satellite communication and navigation system signals. Total electron content (TEC), which is the number of free electrons along the path where the signal is traveling, is a critical quantity that describes the ionosphere and its variability. Modeling and predicting temporal and spatial variations in ionospheric TEC are crucial to ionospheric physics research and ionospheric-based applications (Yao et al., 2018).

Many attempts have been made to specify ionospheric parameters using empirical approaches, because an empirical model can describe the general condition of the ionosphere without actual measured data (Feltens et al., 2011). Several ionosphere empirical models, such as Klobuchar, NeQuick, Standard Plasmasphere Ionosphere Model (SPIM), and International Reference Ionosphere (IRI; Bilitza 2001), are currently available. The IRI is one of the most accepted standard global empirical ionosphere models among others. This model can be used to estimate the values of electron density and temperature, ion temperature and composition, and TEC at altitudes ranging from approximately 50 km to 2000 km at a particular location, time, and day. The IRI model is continuously improved when new data and techniques become available. This model was recently upgraded to the IRI-

2016 version (Bilitza et al., 2017). The model has been improved by ingesting all available data from worldwide ground-based and satellite observations to enhance the model capacity. IRI-2016 includes two new model options for the F2 peak height hmF2 and an enhanced representation of topside ion densities at low and high solar activities. Several small changes were made concerning the use of solar indices and the speedup of the computer program (Bilitza et al., 2017).

The performance of the previous versions of the IRI model in terms of predicting TEC have been investigated to improve the model effectively and provide reference for the application (Maltseva et al., 2012; Scidá et al., 2012; Li et al., 2013; Kenpankho et al., 2013; Okoh et al., 2013; Zakharenkova et al., 2015). Comparative studies with GNSS-derived TEC have validated the performance of different IRI versions over years of varied solar activity in diverse regions. Given the predictability of the diurnal variation of TEC, deficiencies have varied with local time (LT), season, and latitude. After the release of IRI-2016 as the recent version, its performance in predicting TEC has attracted the attention of many researchers (Atici, 2018; Sharma et al.,2018; Tariku, 2018; Jiang et al., 2018). Most existing studies for ionospheric models aimed at the low and middle latitudes. Studies on the TEC prediction performance of different IRI versions worldwide are relatively sparse. Most comparative studies are based on the contrast of the IRI model and global ionospheric map (GIM)- or GNSS-derived TEC. The variations of diurnal and seasonal changes and those in different solar activity years on certain sites have been investigated from several aspects, such as bias, root mean square (RMS) error, and correlation coefficients. Although several assessments of the IRI models have been conducted, few studies on the comprehensive evaluation of the temporal and spatial distribution prediction performance of the IRI model are available. The predictive performance of the IRI model for ionospheric temporal and spatial changes should be evaluated using efficient analytical methods.

Many scholars have recently used the empirical orthogonal function (EOF) decomposition method to analyze the spatial patterns and time temporal variations of the TEC and their relationships with influencing factors (Zhao et al., 2005; Mao et al., 2008; Zhang et al., 2011; Bouya et al., 2012; Zhang et al., 2013; Uwamahoro and Habarulema, 2015; Talaat and Zhu, 2016; Dabbakuti and Ratnam, 2016, 2017; Chang et al., 2017; Andima et al., 2019; Li et al., 2019). The spatial patterns and temporal variations of the TEC are separated by EOF decomposition and can be properly represented by the base functions and associated coefficients, respectively. The data analysis results of a single station and the regional or global TEC indicated that the EOF method is a potentially useful tool for data compression and separation of different physical processes. The EOF method contributes to the comprehensive analysis of the overall spatiotemporal variations in ionospheric TEC.

In this work, GIM TEC data in 2013 were selected as reference values, and the EOF method was introduced to analyze the global TEC prediction performance of IRI-2016. A comparison between the modeled TEC and the reference values was conducted from the perspective of spatial patterns and time variation characteristics. Results provide a reference for the further understanding of the differences between the IRI-2016 and the GIM TECs at a global scale.

2 Data and method

2.1 GIM TEC

The GIM TEC used in this study is the official IGS combined final product provided by the Crustal Dynamic Data Information System (ftp://cddis.gsfc.nasa.gov). Final GIMs are regular products of the International GNSS Service (IGS) since 1998. These GIMs are provided in the ionosphere exchange format with a spatial resolution of 2.5°×5° in geographic latitude and longitude and a temporal resolution of 2 h.

In this study, we downloaded and extracted the 2013 global TEC data from GIMs (referred to as GIM-TEC hereafter).

2.2 IRI-2016

The IRI is the international standard empirical model for terrestrial ionosphere and recommended for international use by the Committee On Space Research and International Union of Radio Science (Bilitza, 2001; Bilitza and Reinisch, 2008; Chauhan and Singh, 2010). The first version was released in 1978, followed by several steadily improved ones in 1986, 1990, 1995, and 2012 (Rawer et al., 1978; Bilitza, 2015). The recent version of this model is IRI-2016 (Bilitza et al., 2016; Bilitza et al., 2017). After IRI-2012, IRI-2016 exhibits the latest improvement in the model by introducing two new F2 peak height hmF2 modeling options with their data sources from ionosonde measurements (Altadill et al., 2013) and COSMIC radio occultations (Shubin, 2015). Hence, this version is independent of the propagation factor M(3000)F2 (Bilitza et al., 2017).

The software package of IRI-2016 can be downloaded from http://irimodel.org/. The IRI software package contains FORTRAN subroutines, model coefficients, index files for IRI-2016 models, README files, and license files. The user can calculate relevant parameters by inputting location, time, height range, model selection, and certain parameters. The global TEC data calculated by using IRI-2016 will be called IRI-TEC hereafter. IRI-TEC can also be calculated online in accordance with http://omniweb.gsfc.nasa.gov/vitmo /iri2016_vitmo.html.

2.3 EOF decomposition

The EOF decomposition analysis method was originally invented by Pearson (1901). This method is performed by using an orthogonal transformation to decompose the original data set into a set of uncorrelated and ordered base functions and associated coefficients.

If an original data matrix X with the dimension M×N is present, then the covariance matrix is determined from the data matrix X in accordance with

$$\Sigma = X^T X \ . \tag{1}$$

The EOF base functions E_i, with i = 1, 2, 3,…, N, are the eigenvectors of the covariance matrix and obtained by solving

$$\Sigma E_i = \lambda_i E_i \ , \tag{2}$$

where λ_i is the associated eigenvalues. Once the EOF base functions are known, the EOF coefficients A_k are obtained using

$$A_k = XE_k \ . \tag{3}$$

The original data set X can be decomposed in terms of the EOF base functions and associated coefficients in accordance with

$$X = \sum_{k=1}^{N} E_k A_k \ . \tag{4}$$

The percentage of the total variance in the data set accounted for by the i th EOF component is given as follows:

$$r_i = 100 \times \frac{\lambda_i}{\sum_{j=1}^{N} \lambda_j} \% , \tag{5}$$

where N denotes the total number of the EOF components accounting for the total variance in the original data set.

Talaat and Zhu (2016) reported that the effectiveness of the EOF technique for TEC is nearly insensitive to the horizontal resolution and length of the data records. We analyzed the global TEC over a 1 year time period (2013) with a 2 h temporal resolution and 37×36 spatial grids.

We first organized the data set $TEC(Lat, Lon, UT, Doy)$ used in this study into a 2D matrix according to location and time epoch, that is, $TEC(epoch, grid)$, where $grid$ is a grid point arranged according to the latitude and longitude, and its total number is 37×36=1332; and $epoch$ is arranged according to Universal Time (UT), with an interval of 2 h. The total epoch number of the study period was 12×365=4380. After performing EOF decomposition, the base function $E_k(grid)$ expressing a spatial pattern and the associated coefficient $A_k(epoch)$ varying with time are obtained.

The EOF method can separate the temporal and spatial variation characteristics. If the IRI TEC and GIM TEC are decomposed separately, it is difficult to directly compare their EOF base functions and coefficients in magnitude. Therefore, we combined the data to form a whole data set for EOF decomposition and compared the two data sets.

The same coefficients of the EOF base function, that is, the same time-varying features, can be obtained by arranging IRI-TEC and GIM-TEC according to the same number of columns. Accordingly, comparing the two data sets' spatial variation features represented by the base functions is feasible.

$$\begin{bmatrix} X_{GIM} \\ X_{IRI} \end{bmatrix} = \sum_{k=1}^{N} \begin{bmatrix} E_{k,GIM} \\ E_{k,IRI} \end{bmatrix} \cdot A_k = \begin{bmatrix} \sum_{k=1}^{N} E_{k,GIM} \cdot A_k \\ \sum_{k=1}^{N} E_{k,IRI} \cdot A_k \end{bmatrix} \tag{6}$$

If IRI-TEC and GIM-TEC are arranged in the same number of rows, then the same spatial variation features represented by EOF base functions will be obtained. Accordingly, the time variation characteristics of the two data sets can be compared.

$$[X_{GIM} \quad X_{IRI}] = \sum_{k=1}^{N} E_k \cdot \begin{bmatrix} A_{k,GIM} & A_{k,IRI} \end{bmatrix} = \begin{bmatrix} \sum_{k=1}^{N} E_k \cdot A_{k,GIM} & \sum_{k=1}^{N} E_k \cdot A_{k,IRI} \end{bmatrix} \tag{7}$$

2.4 Evaluation indicators

In this study, the mean bias was calculated to represent the difference between two data sets. The equation is shown as follows:

$$Bias = \frac{1}{n} \sum_{i=1}^{n} (Y_i - Y_i'), \tag{8}$$

where n is the total number of sample data, and Y_i and Y_i' are sample data for two different data sets. These variables can be TEC from IRI-2016 and GIMs or the values of base functions or coefficients of base functions. The mean relative bias (Bias_rel) can be calculated as follows:

$$\text{Bias\_rel\%} = \frac{1}{n} \sum_{i=1}^{n} \frac{(Y_i - Y_i')}{Y_i'} \times 100. \tag{9}$$

The root mean square (RMS) error of the bias can be calculated using the following expression:

$$RMS = \sqrt{\frac{1}{n} \sum_{i}^{n} (Y_i - Y_i')^2}. \tag{10}$$

The 2D linear correlation coefficient was used to investigate the similarity of the spatial pattern of IRI-TEC and GIM-TEC. The 2D linear correlation coefficient ρ for two matrices A and B with $M \times N$ dimension is calculated as

$$\rho = \sum_{m=1}^{M} \sum_{N=1}^{N} (A_{mn} - \bar{A})(B_{mn} - \bar{B}) \cdot \left[\sum_{m=1}^{M} \sum_{N=1}^{N} (A_{mn} - \bar{A})^2 \right]^{-\frac{1}{2}} \cdot \left[\sum_{m=1}^{M} \sum_{N=1}^{N} (B_{mn} - \bar{B})^2 \right]^{-\frac{1}{2}}, \tag{11}$$

where $\bar{A}$ and $\bar{B}$ are the mean values of matrices A and B, respectively, and they are written as

$$\bar{A} = \frac{1}{MN} \sum_{m=1}^{M} \sum_{n=1}^{N} A_{mn}\text{; and } \bar{B} = \frac{1}{MN} \sum_{m=1}^{M} \sum_{n=1}^{N} B_{mn}. \tag{12}$$

3 Results and analysis

3.1 GIM-TEC and IRI-TEC in 2013

Figure 1 shows the season averages of global GIM-TEC and IRI-TEC at UT 12:00 in 2013. The months are divided into the following four seasons: March equinox (February, March, and April), June solstice (May, June, and July), September equinox (August, September, and October), and December solstice (November, December, and January). The global level of ionospheric TEC at UT 12:00 is lowest during the June solstice compared with that during other seasons. By contrast, the ionospheric TEC reaches the highest level during the December solstice.

The figure illustrates that the spatial distribution characteristics, which change with the latitude and longitude exhibited by IRI-TEC and GIM-TEC, have good consistency. However, the equatorial ionospheric anomaly of IRI-TEC is more pronounced than that of GIM-TEC. The 2D correlation coefficients of the two types of TEC data are shown in Table 1. The correlation coefficients of the four seasons are at least 0.924.

Table 1 reveals that the mean biases between the season averages of global IRI-TEC and GIM-TEC at UT 12:00 are all negative. This result indicates that the TEC level predicted by the IRI-2016 model is lower than that of the GIM. This characteristic can also be seen in Figure 1. The IRI-2016 model provides ionospheric parameters of up to 2000 km and will inaccurately predict the TEC up to GNSS satellites located at an altitude of approximately 20,000 km. The IRI-TEC may be smaller than GIM-TEC because of the missing plasmaspheric content. The mean bias, and mean relative bias between IRI-TEC and GIM-TEC during the December solstice are larger than those in other seasons.

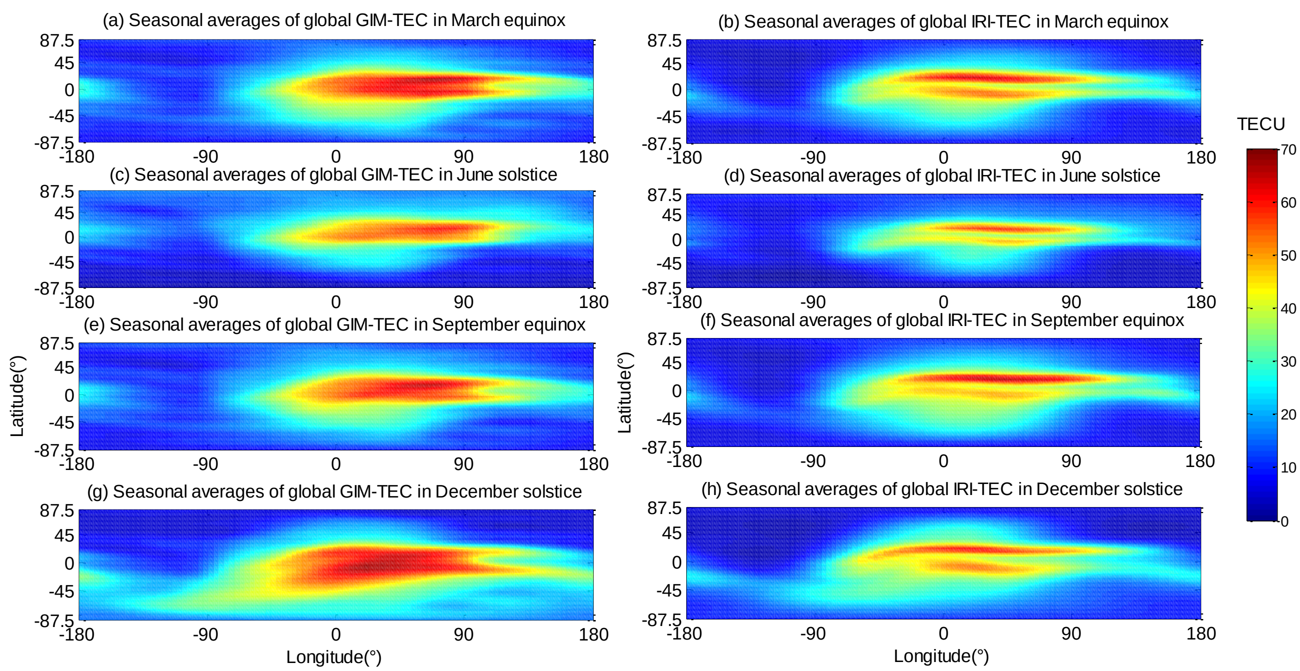

Figure 1. Season averages of global TEC obtained from GIM and IRI at UT 12:00 in 2013. (a) GIM-TEC in the March equinox; (b) IRI-TEC in the March equinox; (c) GIM-TEC in the June solstice; (d) IRI-TEC in the June solstice; (e) GIM-TEC in the September equinox; (f) IRI-TEC in the September equinox; (g) GIM-TEC in the December solstice; and (h) IRI-TEC in the December solstice.

Considering the different levels of ionospheric activities at different latitudes, mean and RMS values of the discrepancies between seasonal averages of GIM-TEC and IRI-TEC over different latitudinal regions in 2013 were calculated. Results are shown in Figure 2. From Figure 2, the mean and RMS values over the area near the equator generally exhibit peak values. GIM-TEC values over the equator and low latitudes are much larger than IRI-TEC values, especially over the ionospheric trough near the magnetic equator shown in Figure 1. The mean and RMS values over Southern Hemisphere during the December solstice are significantly large, and they are also very large over Northern Hemisphere during the June solstice. Therefore, there are large discrepancies between GIM-TEC and IRI-TEC over the summer Hemisphere.

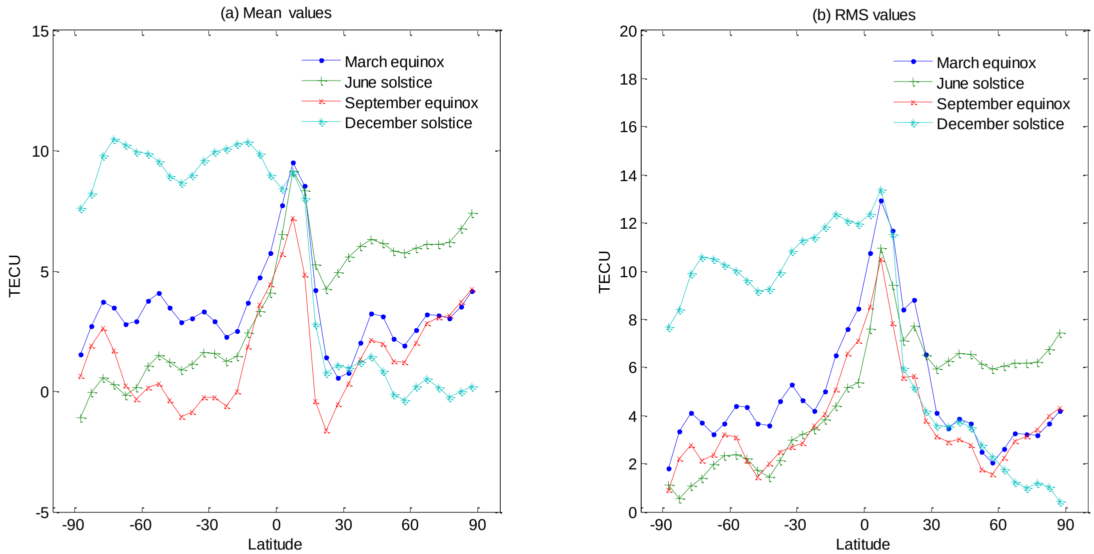

Figure 2. Mean and RMS values of the discrepancies between GIM-TEC and IRI-TEC at different latitudes during four seasons. The gridded values of the global IRI-TEC and GIM-TEC at different UTs for each day of the year 2013 were used to calculate the daily RMS. Results are shown in Figure 3, which also displays the daily solar F10.7 index and daily average of geomagnetic AE index in 2013. The solar F10.7 and geomagnetic AE indexes are available at https://omniweb.gsfc.nasa.gov/form/dx1.html. Figure 3 demonstrates that the daily RMS of the differences between global IRI-TEC and GIM-TEC is in good agreement with the daily solar F10.7 index. The correlation coefficients between the RMS and the solar F10.7 or geomagnetic AE index are 0.78 and −0.19, respectively. Results indicate that the ionospheric TEC prediction error of the IRI-2016 model presents a strong correlation with solar activity.

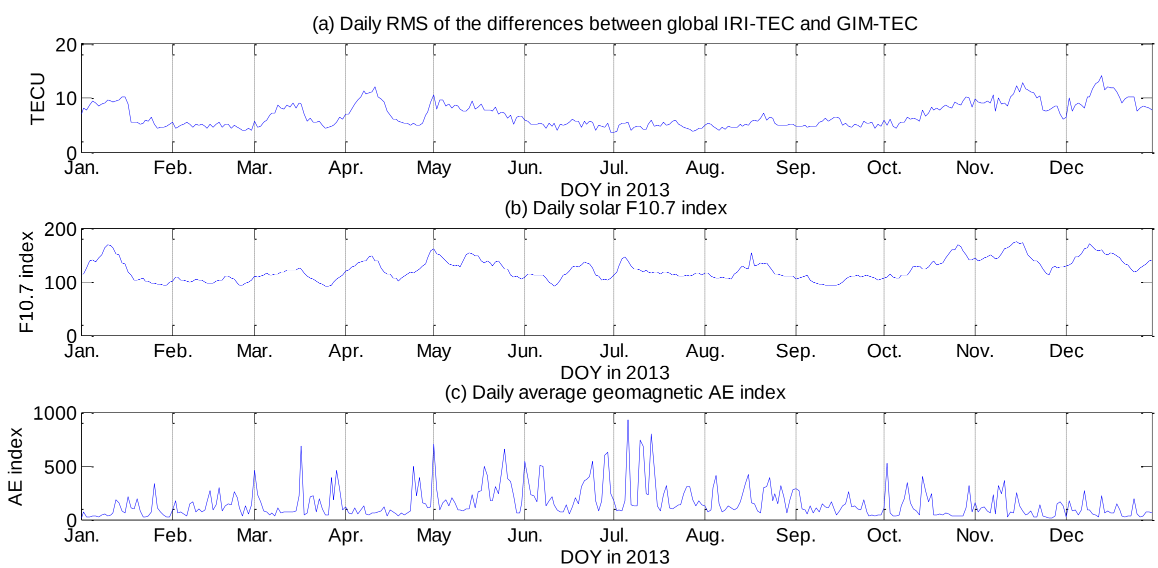

Figure 3. Daily (a) RMS of the differences between global IRI-TEC and GIM-TEC, (b) solar F10.7 index, and daily (c) average geomagnetic AE index in 2013.

Table 1. Correlation coefficient and bias statistics among the season averages of global IRI-TEC and GIM-TEC at UT 12:00 in 2013

	Correlation coefficient ρ	Maximum bias (TECU)	Minimum bias (TECU)	Mean bias (TECU)	Mean relative bias Bias_rel%
March equinox	0.944	16.199	−23.332	−3.456	−20.0%
June solstice	0.948	7.7401	−20.478	−3.7193	−19.8%
September equinox	0.953	12.476	−20.525	−1.569	−11.0%
December solstice	0.924	14.866	−27.728	−5.743	−23.1%

3.2 Differences of spatial patterns between IRI-TEC and GIM-TEC based on the same time-varying characteristics

We combined the IRI-TEC and GIM-TEC data to obtain the same TEC time-varying characteristics using Eq. (6) and analyzed their differences in terms of spatial patterns.

The time-varying characteristics are reflected in the coefficient A_k of the EOF decomposition. Given that the TEC data are in accordance with the 2 h time interval, coefficient A_k is also the data that vary with the 2 h time interval. We described the coefficients of the base function according to the changes in UT and day of year (DOY) in Figure 4 to reflect the seasonal changes effectively.

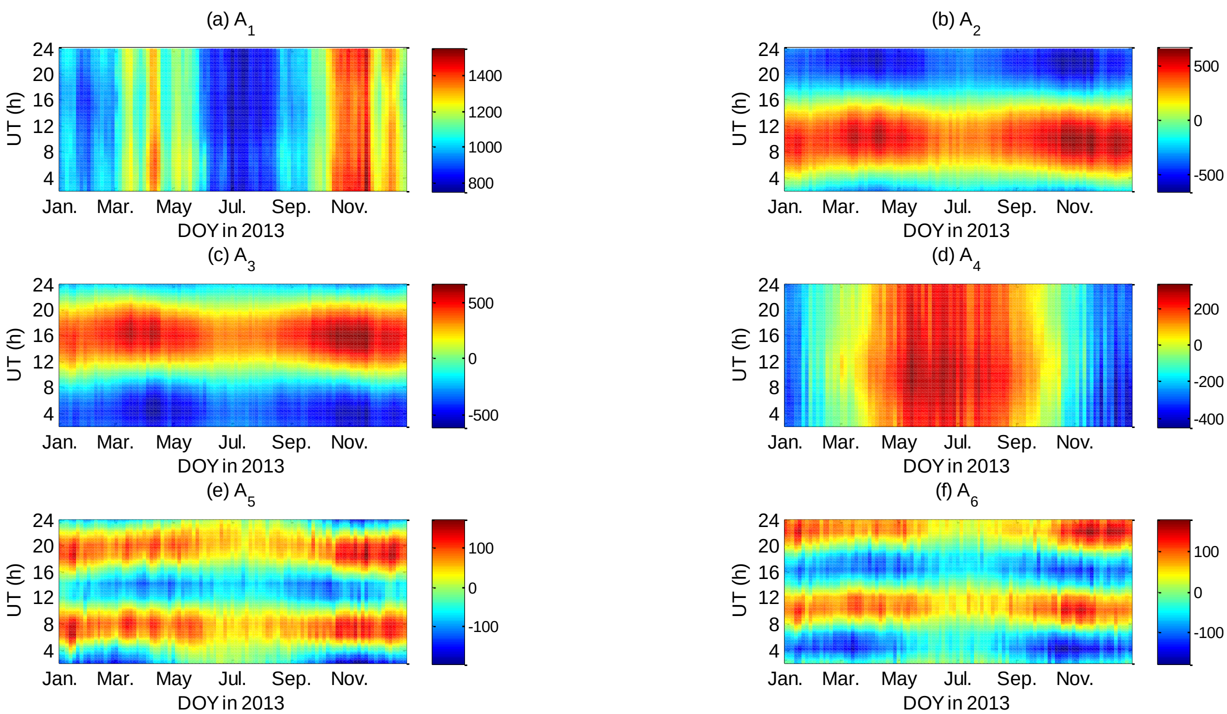

Figure 4. Associated coefficients $A_1 - A_6$ of the first six orders of EOF base functions based on Eq. (6), and $A_1 - A_6$ were plotted against UT and DOY.

The main EOF base functions extracted from Eq. (6) are shown in Figure 5. The graphics in the left column of Figure 5 exhibit the first six base functions E_i of GIM-TEC, whereas those in the right column of Figure 5 depict the base functions of IRI-TEC.

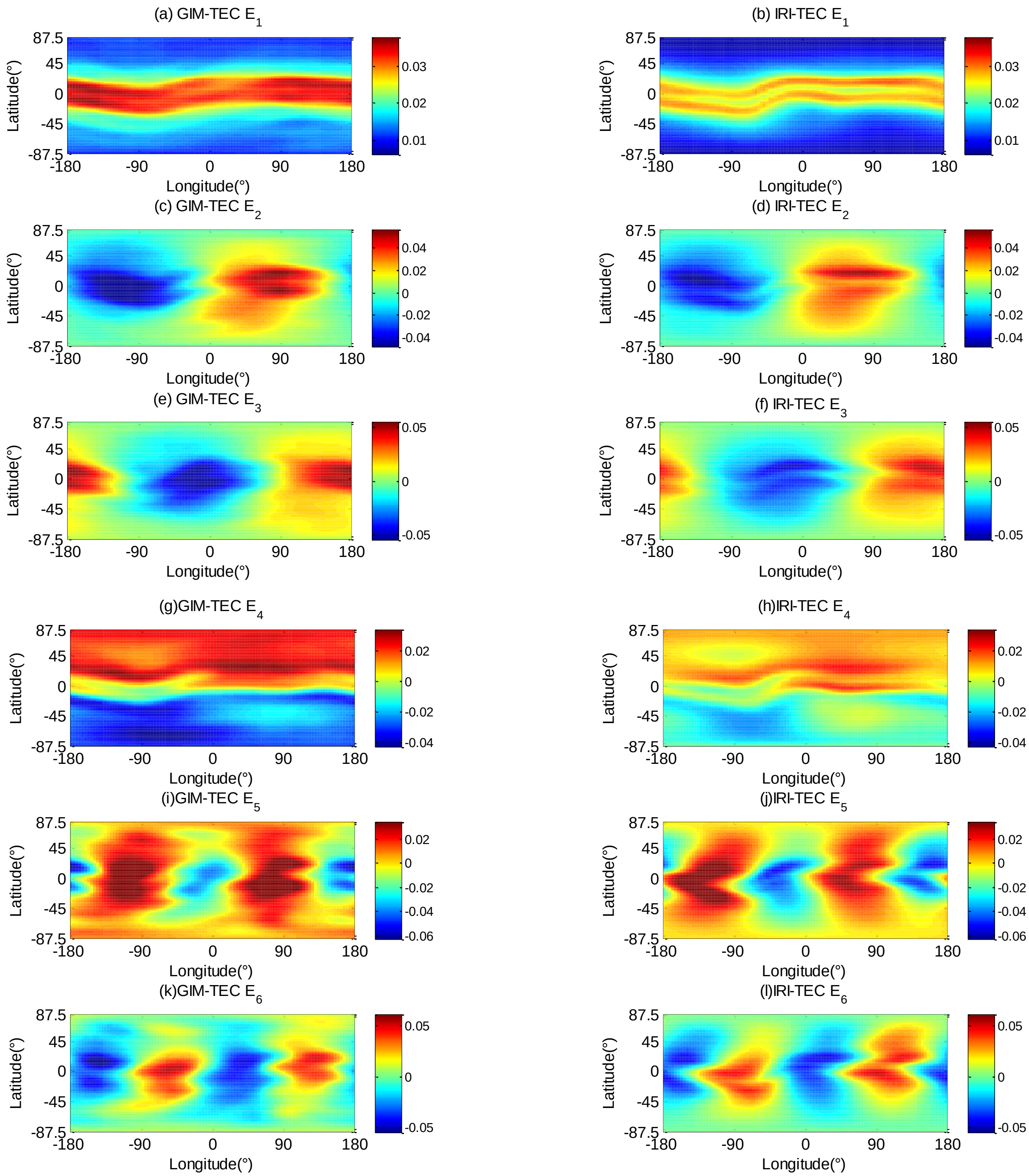

Figure 5. First six orders of EOF base functions $E_1 - E_6$ extracted on the basis of Eq. (6). The figures in the left column are the base functions of GIM-TEC, and those in the right column are the base functions of IRI-TEC.

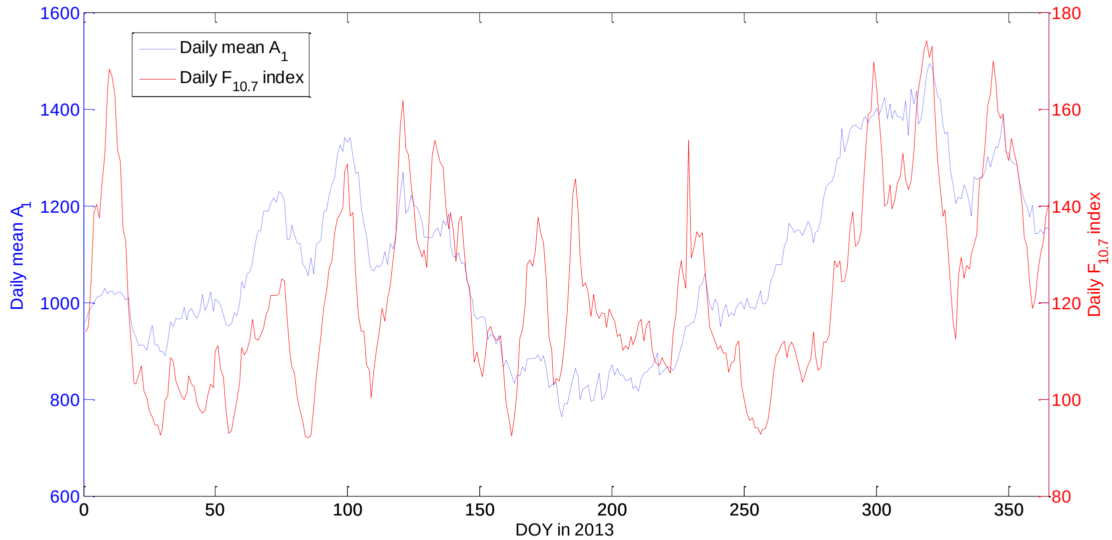

Figure 6. Daily mean first EOF coefficient A_1 and daily solar F10.7 index.

The first base function E_1 of GIM-TEC and IRI-TEC in Figs. 5(a) and (b) describe the overall average of global TEC. This function reflects the daily average effect of solar forcing and offset magnetic field (Talaat and Zhu, 2016). The TEC over the area near the geomagnetic equator exhibits a peak value. The TEC value decreases with the increase in geomagnetic latitude. The spatial distribution characteristics of E_1 of the two models are very consistent. However, the peak GIM-TEC value over the geomagnetic equator is greater than that of the IRI-TEC. The ionospheric trough near the geomagnetic equator is evident in Figure 5(b). The daily mean A_1 and solar F10.7 index are illustrated in Figure 6, which shows that these two data sets demonstrate a consistent trend. The correlation coefficient between daily mean A_1 and F10.7 index is 0.61. Solar activity is the primary determinant of the first base function E_1.

Figs. 5(c)–(f) present that the second and third base functions reflect the spatial distribution that varies along the longitude direction. The two base functions E_2 and E_3 approximately have the same magnitude and show a phase shift of π/2, which is consistent with the results of Talaat and Zhu (2016). These functions reflect the change of diurnal solar radiation as it changes with the LT. This change of GIM-TEC and IRI-TEC is generally consistent; their main difference is reflected in the peak region of the equator, and GIM-TEC shows large peak values. The EOF coefficients A_2 and A_3 corresponding to Figs. 4(b) and (c) show the change of the diurnal variation, and a change characteristic of the semiannual period is observed. The levels of A_2 and A_3 during equinox seasons are larger than those during solstice seasons.

The fourth base function E_4 reflects interhemispheric asymmetry, which is mainly caused by the seasonal variation of the inclination angle of the Earth's orbit. A_4 in Figure 4(d) indicates the seasonal variation of the interhemispheric asymmetry of the TEC and a strong annual cycle. The TEC component corresponding to base function E_4 in the Southern Hemisphere is positive. In the Northern Hemisphere, the maximum value of the E_4 component is on DOY150, whereas that in the Southern Hemisphere is on DOY347.

Similar to E_2 and E_3, the fifth and sixth base functions E_5 and E_6 also reflect the spatial distribution characteristics along the longitude (Figs. 5(i) to (l)). In conjunction with Figs. 4(e) and (f), these two base functions have semidiurnal period changes, and the phases of the two base functions differ by π/4 and are of approximately equal magnitude. Base functions E_5 and E_6

represent a semidiurnal variation that changes with LT, and their coefficients A_5 and A_6 show a semiannual period. The intensity of the semidiurnal variation is strong during the equinox season and weak during the June solstice.

We calculated the variances, correlation coefficients, biases, and their relative biases to analyze the spatial distribution characteristics of GIM-TEC and IRI-TEC. The statistical results are shown in Table 2, which indicates that the base functions of the two data sets are correlated and present good consistency with Figure 5.

Table 2. Variances of the base function, correlation coefficient, and bias statistics among the base functions of GIM-TEC and IRI-TEC

Base function	E_1	E_2	E_3	E_4	E_5	E_6
Variances r_i	79.03%	8.24%	7.52%	2.55%	0.37%	0.35%
Correlation coefficient ρ	0.971	0.960	0.956	0.936	0.739	0.716
Maximum bias	0.0022	0.0189	0.0192	0.0276	0.0481	0.0587
Minimum bias	−0.0105	−0.0217	−0.0243	−0.0300	−0.0528	−0.0586
Mean bias	−0.0035	−0.00092	−0.00056	0.00095	−0.00593	0.00068
Mean relative Bias Bias_rel%	−20.8%	−12.3%	−4.2%	−56.7%	−34.4%	−18.2%

We showed the difference between the six base functions of GIM-TEC and IRI-TEC in Figure 7 to have an intuitive understanding of the difference between the IRI and the GIM base functions.

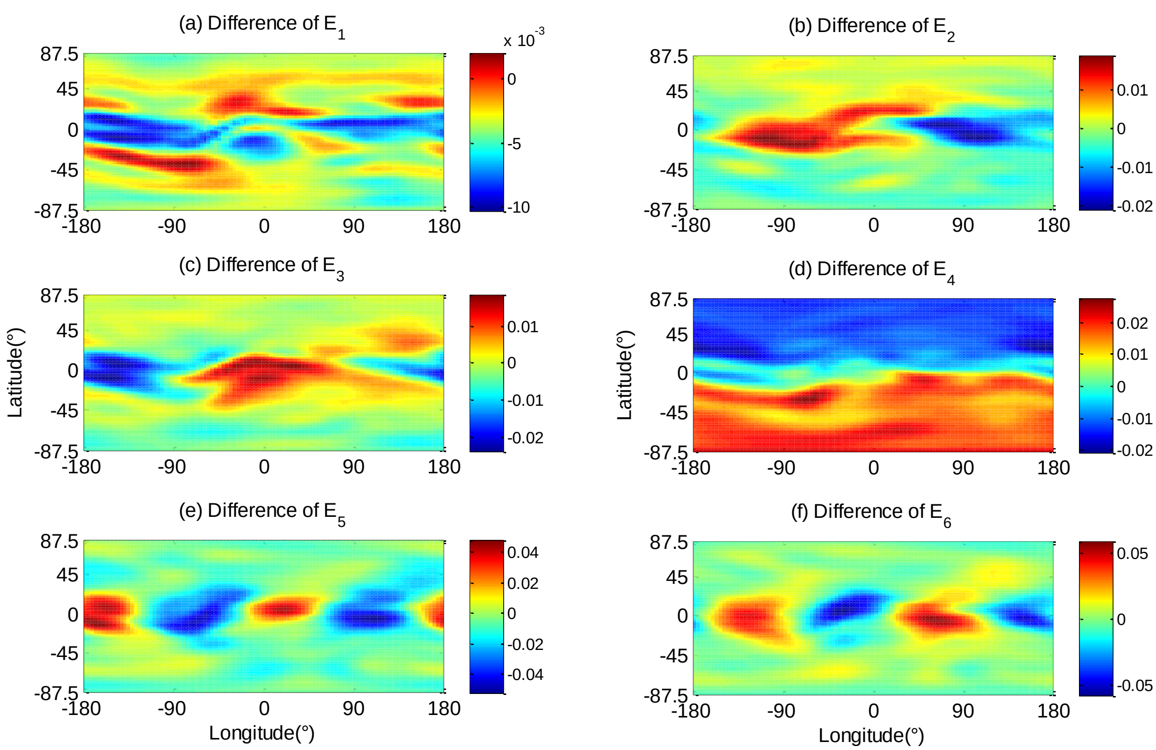

Figure 7. Differences of the first six orders of the base functions of GIM-TEC and IRI-TEC.

Figure 7 shows that the differences of other modes exhibit a large deviation in the equatorial and low latitude regions, except for the interhemispheric asymmetry feature E_4. The magnitudes of the spatial distribution changes of the IRI-TEC for all six base functions are significantly smaller than those of GIM-TEC.

The mean relative bias statistics of the base functions of GIM-TEC and IRI-TEC in Table 2 are negative. This finding indicates that the spatial variations of the base functions of IRI-TEC are generally underestimated compared with those of GIM-TEC. Here, the mean relative bias of E_4 reached −56%, and the underestimation is serious. This outcome is consistent with the statistical results in Table 1.

3.3 Differences of time-varying characteristics between IRI-TEC and GIM-TEC based on the same spatial patterns

Eq. (7) shows that the same EOF base functions are extracted for GIM-TEC and IRI-TEC. The differences of the corresponding coefficients of the EOF base functions between GIM-TEC and IRI-TEC are then compared, and those of their time variation characteristics can be analyzed.

Figure 8 shows the six EOF base functions extracted in accordance with Eq. (7). Similar to the EOF base function extracted in Figure 5, the first base function is consistent with the average variation of the TEC, varying with geomagnetic latitude. The second and third base functions are related to the diurnal variation of solar radiation change with longitude due to the LT. The fourth base function reflects the interhemispheric asymmetry caused by the seasonal variation of the inclination angle of the Earth's orbit. The fifth and sixth base functions reflect the characteristics of the semidiurnal variation with longitude due to the LT.

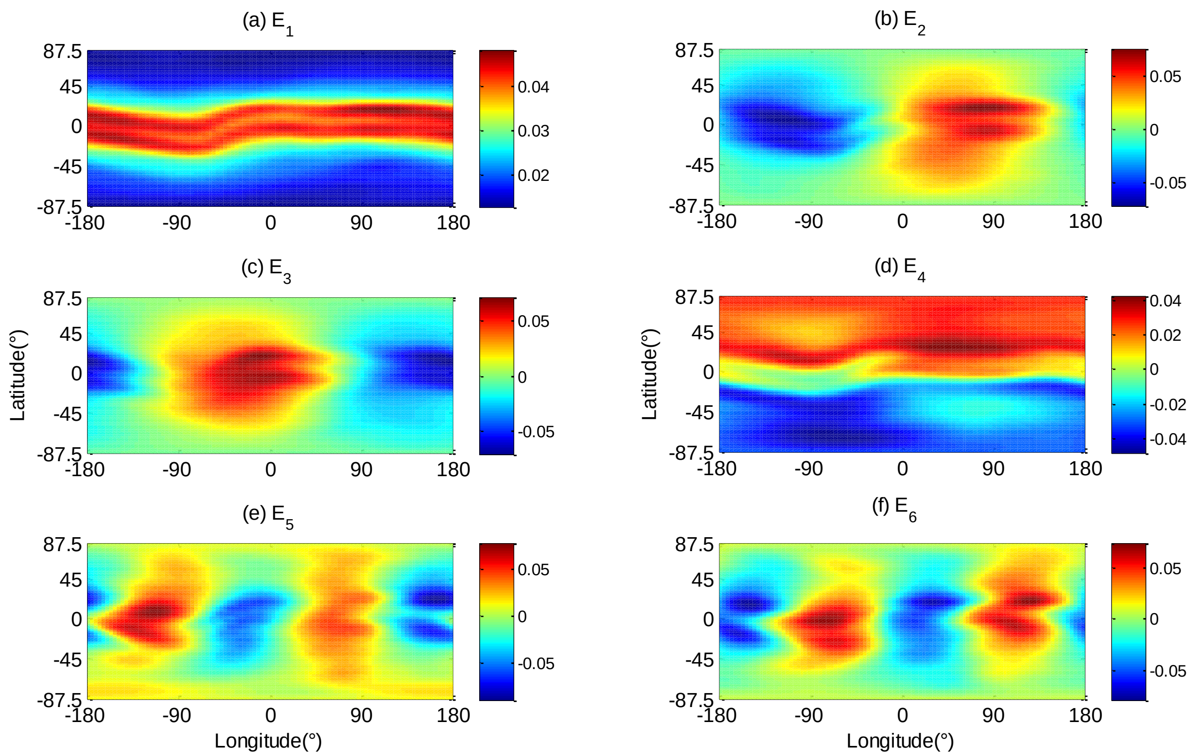

Figure 8. Six EOF base functions $E_1 - E_6$ extracted in accordance with Eq. (7).

The coefficients of the different base functions of GIM-TEC and IRI-TEC obtained in accordance with Eq. (7) are shown in Figure 9.

The time-varying characteristics of the coefficients in Figure 9 are very consistent with the results shown in Figure 4. From Figs. 9(a) and (b), the variations of A_1 are mainly related to solar activity, and solar activity is the primary determinant of the first base function E_1 in Figure 8(a), which describes the overall average of global TEC. From Figs. 9(c)–(f), the EOF coefficients A_2 and A_3 of GIM-TEC and IRI-TEC all obviously exhibit a diurnal period and a semiannual period. They reflect the diurnal variation of solar radiation change with longitude due to the LT. A_4 in Figs. 9(g) and (h) indicate a strong annual cycle variation of the interhemispheric asymmetry of the TEC. A_5 and A_6 show a semiannual period of the base functions E_5 and E_6, which represent a longitudinal variation that changes with LT. The EOF coefficients of GIM-TEC and IRI-TEC have consistent annual, semiannual, diurnal, and semidiurnal variations. Therefore, Figure 9 manifests that GIM-TEC and IRI-TEC have highly consistent temporal variation characteristics based on the same spatial distribution modes E_k according to equation (7). The variance and correlation coefficients of $A_1 - A_6$ of the two types of data and the bias statistics of such coefficients are shown in Table 3.

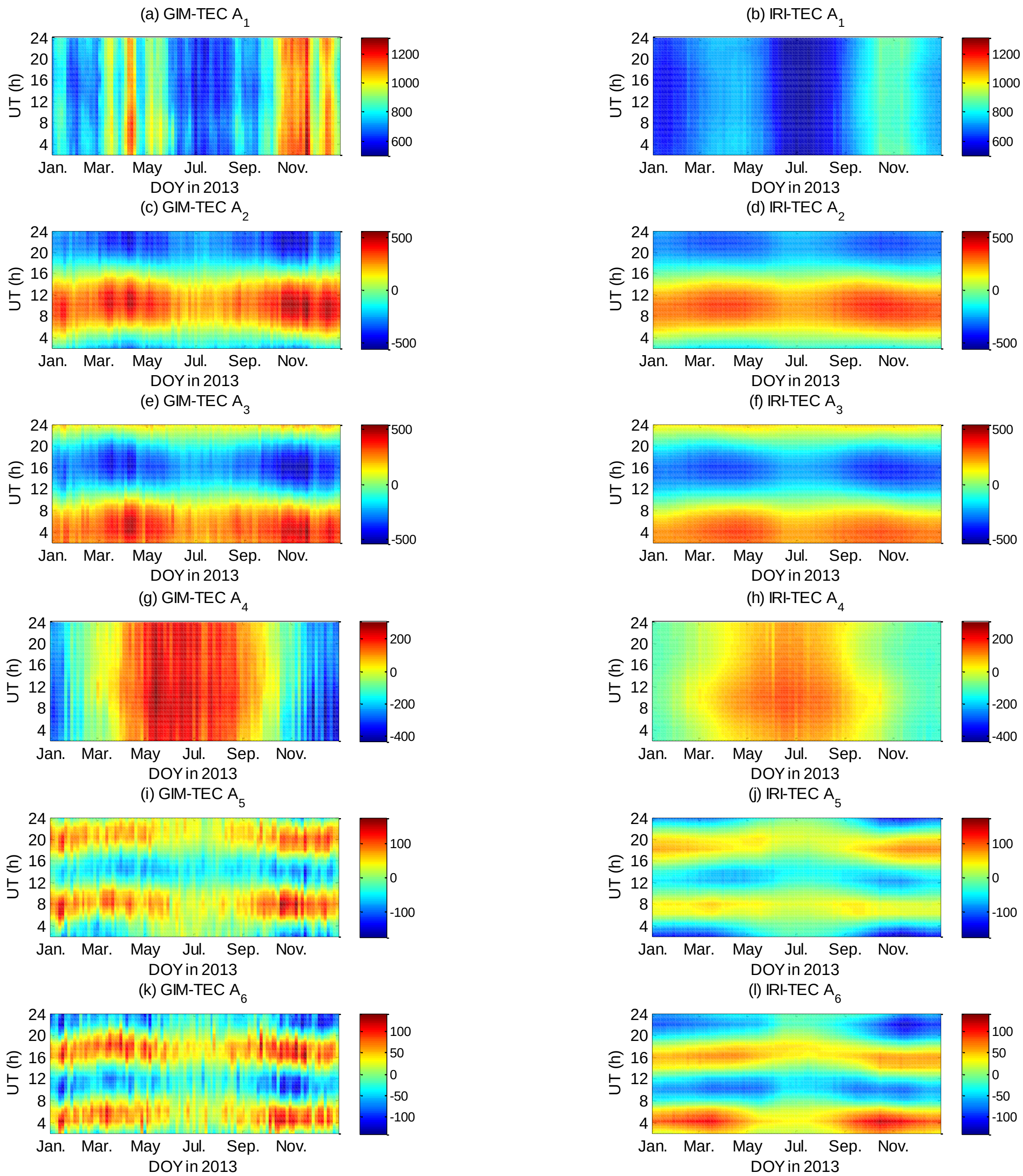

Figure 9. Associated coefficients $A_1 - A_6$ of the EOF base functions extracted in accordance with Eq. (7).

Table 3. Variances of base function, correlation coefficient, and bias statistics among coefficients $A_1 - A_6$ of GIM-TEC and IRI-TEC

Coefficient	A_1	A_2	A_3	A_4	A_5	A_6
Variances of base function r_i	79.03%	8.24%	7.52%	2.55%	0.37%	0.35%
Correlation coefficient	0.806	0.974	0.972	0.949	0.634	0.725

ρ						
Maximum bias	118.24	252.39	246.44	323.55	112.84	143.39
Minimum bias	−465.34	−204.87	−224.75	−222.50	−165.46	−101.54
Mean bias	−129.78	8.33	13.53	−25.43	−26.89	2.98
Mean relative bias Bias_rel%	−16.94%	−10.62%	−10.98%	−52.83%	−38.82%	−17.98%

The magnitudes of coefficients $A_1 - A_6$ of IRI-TEC are generally smaller than those of the GIM-TEC, especially for A_4. The maximum and minimum values of GIM-TEC A_4 in Figure 9(g) are 302.27 and −431.47, respectively. The variation range of the IRI-TEC A_4 in Figure 9(h) is −138.99 to 165.13. Results in Table 3 indicate that A_4 exhibits the largest mean relative bias.

Figure 9 shows that $A_1 - A_6$ reflect the time-varying characteristics of different scales. We conducted EOF decomposition on $A_1 - A_6$ according to the following equation to divide their diurnal and seasonal variation characteristics:

$$A_i(UT, Doy) = \sum_{k=1}^{N} E_{ik}(UT) \times A_{ik}(Doy)\,, \qquad (13)$$

where A_i represents the coefficient of the i th order the EOF base function. This part is the second-layer EOF decomposition in this study.

Eq. (13) shows that the time-varying feature E_{ik} depending on UT and seasonal variation A_{ik} can be obtained. Given that the first base function and corresponding coefficient usually demonstrates the main variation, the decomposed first base function E_{i1} and associated coefficient A_{i1} are shown in Figure 10.

The left column of Figure 10 manifests base function E_{ik}, which represents the diurnal variation characteristic of the base function E_i. The coefficients of the second-layer EOF decomposition A_{i1} represent the variations in long time scales. A_{i1} is shown in the right column of Figure 10. Previous studies have shown that the long time-scale variations of TEC are mainly influenced by solar and geomagnetic activities and periodical variation. The solar F10.7 index is also shown in the right column of Figure 10 together with A_{i1}.

The first base function E_1 in Figure 8(a) describes the overall average global TEC, and Figure 10(a) shows E_{11}, the diurnal variation characteristic of E_1. GIM-TEC and IRI-TEC have similar magnitudes, whereas the diurnal variation of IRI-TEC is insignificant. A_{11} of GIM-TEC and IRI-TEC in Figure 10(b) shows a pronounced semiannual period. However, A_{11} of GIM-TEC in most days are larger than those of IRI-TEC, and the correlation between F10.7 index and A_{11} of GIM-TEC is evidently observed.

As shown in Figs. 10(c), (e), and (g), the diurnal variations of the second, third, and fourth base functions $E_2 - E_4$ of GIM-TEC and IRI-TEC show minimal discrepancy. Hence, the IRI-2016 model accurately captures the diurnal variations of the solar radiation according to LT and interhemispheric asymmetry.

A_{21} and A_{31} of GIM-TEC and IRI-TEC are shown in Figs. 10(d) and (f). These functions evidently demonstrate a semidiurnal variation period. A_{21} and A_{31} of IRI-TEC during the equinox season are lower than those of GIM-TEC. The correlation between F10.7 index and A_{21} and A_{31} of GIM-TEC is also observed. A_{41} of GIM-TEC and A_{41} of IRI-TEC in Figure 10(h) exhibit an evident annual period variation of interhemispheric asymmetry. However, the summer-to-winter annual variation of GIM-TEC is much larger than that of IRI-TEC.

The fifth and sixth base functions E_5 and E_6 in Figs. 8(e) and (f) reflect the spatial distribution characteristics along the longitude due to LT. E_{51} and E_{61} in Figs. 10(i) and (k) represent a semidiurnal variation. However, shifts in the peak value time between GIM-TEC and IRI-TEC are detected in E_{51} and E_{61}. A_{51} and A_{61} in Figs. 10(j) and (l) exhibit a semiannual variation, and A_{51} and A_{61} of GIM-TEC are relatively consistent with those of IRI-TEC.

We calculated the correlation coefficients between A_{i1} of GIM-TEC and solar F10.7 index. Results are shown in Table 4. Coefficients A_{11}, A_{21}, and A_{31} are highly related to solar activity.

Table 4. Correlation coefficients between A_{i1} of GIM-TEC and solar F10.7 index

Coefficient	A_{11}	A_{21}	A_{31}	A_{41}	A_{51}	A_{61}
Correlation coefficient	0.715	0.559	0.563	−0.301	0.423	0.438

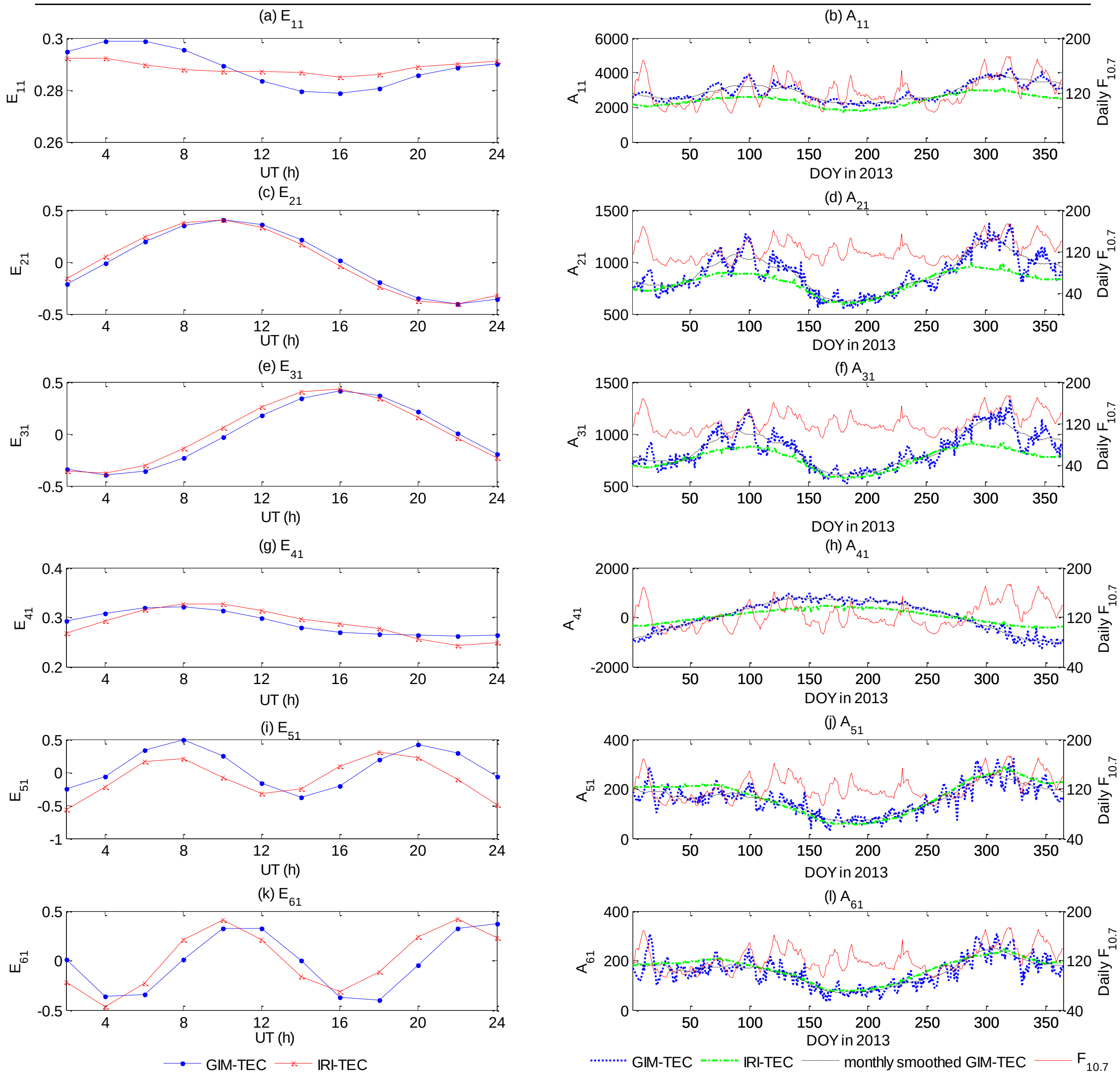

Figure 10. First base function E_{i1} and associated coefficient A_{i1} of the six coefficients $A_1 - A_6$ according to Eq. (12). The monthly smoothed A_{i1} of GIM-TEC and daily solar F10.7 index are shown together with A_{i1}.

$A_{11} - A_{61}$ in Figure 10 show that IRI-TEC mainly reflects the annual and semiannual variations of the ionospheric TEC. The monthly and short period variations with solar activity are unrepresented by IRI-TEC.

Although the IRI-TEC will be smaller than the GIM-TEC because of the missing plasmaspheric content, A_{11} of IRI-TEC in Figure 10(b) shows a quite large underestimation compared with that of GIM-TEC. The strong correlation between A_{11} of GIM-TEC and solar activity is unrepresented by A_{11} of IRI-TEC. The diurnal variation of the first base function of GIM-TEC represented by E_{11} is partially represented by E_{11} of IRI-TEC. The variance contribution rate of the first EOF component reaches 79.03%; thus, the influence of its coefficient is large for the deviation of IRI-TEC and GIM-TEC.

4. Conclusion

In this study, the global TEC prediction performance of the IRI-2016 model was evaluated. The EOF decomposition method was introduced to compare the global TEC data from the IRI-2016 model and GIMs in 2013. The prediction performance of the IRI-2016 model could be evaluated from two perspectives, namely, spatial pattern and temporal variation. The main conclusions are as follows:

1. A general underestimation of the IRI-2016 model can be observed compared with the season averages of global GIM-TEC in 2013, and the RMS of the global TEC deviation is strongly correlated with the solar activity F10.7 index.

2. The six base functions extracted by performing EOF decomposition on the global TEC data from IRI-2016 and GIMs include the following: the variation with the geomagnetic latitude reflecting the daily averaged solar forcing, the diurnal and semidiurnal periodic changes with longitude due to local time, and the interhemispheric asymmetry caused by the annual variation of the inclination angle of the Earth's orbit. The spatiotemporal features extracted from IRI-TEC and GIM-TEC data have good consistency. The IRI-2016 model follows the variation patterns of the observed GIM-TEC.

3. The spatial variation characteristics of IRI-TEC and GIM-TEC can be extracted for comparison on the basis of the same EOF coefficients. Results show that the spatial distribution fluctuation of the IRI-TEC is smaller than that of GIM-TEC. The average relative deviation of the base function representing the interhemispheric asymmetry reaches −56.7%. The interhemispheric asymmetry presents a relatively stable deviation between IRI-TEC and GIM-TEC. The other spatial distribution variations have large deviations in the equator and low latitudes.

4. The temporal variation characteristics of IRI-TEC and GIM-TEC are extracted and compared on the basis of the same EOF base functions. The degree of IRI-TEC changes with time is weaker than that of GIM-TEC. The average relative deviation of the fourth base function coefficient reaches −52.83%. Most diurnal, annual, and semiannual variations of the six base functions of IRI-TEC are consistent with those of GIM-TEC. However, the change with solar activity is unrepresented by IRI-TEC. The diurnal variation of the first base function and the annual variation of the fourth base function have a relatively large deviation between IRI-TEC and GIM-TEC.

5. Results of the spatial and temporal variation characteristic analyses show that the deviation of the first and fourth EOF components between IRI-TEC and GIM-TEC are the two main influencing factors.

Data availability. The data used in this study were downloaded from ftp://cddis.gsfc.nasa.gov/ (last accessed: 10 April 2019), http://irimodel.org/ (last accessed: 12 March 2019), and https://omniweb.gsfc.nasa.gov/ (last accessed: 21 April 2019).

Author contribution. SL contributed to the conception of the study. SL and JX contributed significantly to the data analysis and manuscript preparation. HZ and JZ performed the model validation and wrote part of the manuscript. ZX and MX contributed to some data analysis work.

Competing interests. The authors declare that they have no conflict of interest.

Acknowledgments. This work is supported by the Fundamental Research Funds for the Central Universities (Grant Numbers: 2652017105), and the National Natural Science Foundation of China (Grant Number 41574011).

References

A, E., Zhang, D., Xiao, Z., Hao Y., Ridley, A. J., and Moldwin, M.: Modeling ionospheric foF2 by using empirical orthogonal function analysis, Ann. Geophys., 29, 1501-1515, 2011.

Altadill, D., Magdaleno, S., Torta, J. M., Blanch, E.: Global empirical models of the density peak height and of the equivalent scale height for quiet conditions, Adv. Space Res., 52, 1756–1769, https://doi.org/10.1016/j.asr.2012.11.018, 2013.

Andima, G., Amabayo, E. B., Jurua, E., and Cilliers, P. J.: Modeling of GPS total electron content over the African low-latitude region using empirical orthogonal functions, Ann. Geophys., 37, 65-76, https://doi.org/10.5194/angeo-37-65-2019, 2019.

Atici, R.: Comparison of GPS TEC with modelled values from IRI 2016 and IRI-PLAS over Istanbul, Turkey, Astrophys. Space Sci., 363-231, https://doi.org/10.1007/s10509-018-3457-0, 2018.

Bilitza, D.: International Reference Ionosphere 2000, Radio Sci., 36, 261-275, https://doi.org/10.1029/2000RS002432, 2001.

Bilitza, D.: The International Reference Ionosphere-Status 2013, Adv. Space Res., 5, 1914-1927, https://doi.org/10.1016/j.asr.2014.07.032, 2015.

Bilitza, D., Altadill, D., Truhlik, V., Shubin, V., Galkin, I., Reinisch, B., and Huang, X.: International Reference Ionosphere 2016: from ionospheric climate to real-time weather predictions, Space Weather, 15, 418-429, 2017.

Bilitza, D. and Reinisch, B. W.: International Reference Ionosphere 2007: Improvements and new parameters, Adv. Space Res., 42, 599-609, https://doi.org/10.1016/j.asr.2007.07.048, 2008.

Bilitza, D., Watanabe, S., Truhlik, V., and Altadill, D.: IRI-2016: Description and Introduction, Abstract submitted for 41st COSPAR Scientific Assembly, July, Istanbul, Turkey, 2016.

Bouya, Z., Terkildsen, M., Francis, M., and Neudegg, D.: EOF Analysis applied to Australian Regional Ionospheric TEC modelling, AOSWA, 22-24 February, Chiang Mai, Thailand, 2012.

Chang, X., Zou, B., Guo, J., Zhu, G., Li, W., and Li, W.: One sliding PCA method to detect ionospheric anomalies before strong Earthquakes: Cases study of Qinghai, Honshu, Hotan and Nepal earthquakes, Adv. Space Res., 59, 2058-2070, https://doi.org/10.1016/j.asr.2017.02.007, 2017.

Chauhan,V. and Singh, O. P.: A morphological study of GPS-TEC data at Agra and their comparison with the IRI model, Adv. Space Res., 46, 280-290, https://doi.org/10.1016/j.asr.2010.03.018, 2010.

Dabbakuti, J. R. K. K. and Ratnam, D. V.: Characterization of ionospheric variability in TEC using EOF and wavelets over low-latitude GNSS stations, Adv. Space Res., 57, 2427-2443, https://doi.org/10.1016/j.asr.2016.03.029, 2016.

Dabbakuti, J. R. K. K. and Ratnam, D. V.: Modeling and analysis of GPS-TEC low latitude climatology during the 24th solar cycle using empirical orthogonal functions, Adv. Space Res., 60, 1751-1764, https://doi.org/10.1016/j.asr.2017.06.048, 2017.

Feltens, J., Angling, M., Jackson-Booth, N., Jakowski, N., Hoque, M., HernándezPajares, M., Aragón, Á., María, Á., and Orús-Pérez, R.: Comparative testing of four ionospheric models driven with GPS measurements, Radio Sci., 46, RS0D12, https://doi.org/10.1029/2010RS004584, 2011.

Gulyaeva, T. L. and Bilitza, D.: Towards ISO standard Earth ionosphere and plasmasphere model, In: New Developments in the Standard Model, NOVA Publishers, https://www.novapublishers. com/catalog/product_info.php?products_id=35812, 2012.

Jiang, H., Liu, J., Wang, Z., An, J., Ou, J., Liu, S., and Wang, N.: Assessment of spatial and temporal TEC variations derived from ionospheric models over the polar regions, J. Geodesy, 93, 455-471. https://doi.org/10.1007/s00190-018-1175-6, 2019.

Kenpankho, P., Supnithi, P., and Nagatsuma, T.: Comparison of observed TEC values with IRI-2007 TEC and IRI-2007 TEC with optional foF2 measurements predictions at an equatorial region, Chumphon, Thailand, Adv. Space Res., 52, 1820-1826, https://doi.org/10.1016/j.asr.2013.08.012, 2013.

Li, S., Li, L., and Peng, J.: Variability of Ionospheric TEC and the Performance of the IRI-2012 Model at the BJFS Station, China, Acta Geophys., 64, 1970-1987, 2016.

Li, S., Zhou, H., Xu, J., Wang, Z., Li, L., and Zheng, Y.: Modeling and analysis of ionosphere TEC over China and adjacent areas based on EOF method, Adv. Space Res., https://doi.org/10.1016/j.asr.2019.04.018, 2019.

Maltseva, O. A., Mozhaeva, N. S., Poltavsky, O. S., and Zhbankov, G. A.: Use of TEC global maps and the IRI model to study ionospheric response to geomagnetic disturbances, Adv. Space Res., 49, 1076-1087, https://doi.org/10.1016/j.asr.2012.01.005, 2012.

Mao, T., Wan, W., Yue, X., Sun, L., Zhao, B., and Guo, J.: An empirical orthogonal function model of total electron content over China, Radio Sci., 43, RS2009, https://doi.org/10.1029/2007RS003629, 2008.

Okoh, D., McKinnell, L., Cilliers, P., and Okeke, P.: Using GPS-TEC data to calibrate VTEC computed with the IRI model over Nigeria, Adv. Space Res., 52, 1791-1797, https://doi.org/10.1016/j.asr.2012.11.013, 2013.

Pearson, K.: On lines and planes of closest fit to systems of points in space, Philos. Mag., 2, 559-572, 1901.

Rawer, K., Ramakrishnan, S., and Bilitza, D.: International Reference Ionosphere 1978. International Union of Radio Science, URSI Special Report, pp.75, Bruxelles, Belgium, 1978.

Scidá, L. A., Ezquer, R. G., Cabrera, M. A., Mosert, M., Brunini, C., and Buresova, D.: On the IRI 2007 performance as a TEC predictor for the South American sector, J. Atmos. Sol. Terr. Phys., 81-82, 50-58, https://doi.org/10.1016/ j.jastp.2012.04.001, 2012.

Sharma, S. K., Ansari, K., and Panda, S. K.: Analysis of Ionospheric TEC Variation over Manama, Bahrain, and Comparison with IRI-2012 and IRI-2016 Models, Arab. J. Sci. Eng., 43, 3823-3830, 2018.

Shubin, V. N.: Global median model of the F2-layer peak height based on ionospheric radio-occultation and ground-based Digisonde observations, Adv. Space Res., 56, 916–928, https://doi.org/10.1016/j.asr.2015.05.029, 2015.

Talaat Elsayed, R. and Zhu, X.: Spatial and temporal variation of total electron content as revealed by principal component analysis, Ann. Geophys., 34, 1109-1117, 2016.

Tariku, Y. A.: Assessment of improvement of the IRI model over Ethiopia for the modeling of the variability of TEC during the period 2013-2016, Adv. Space Res., 63, 1634-1645, https://doi.org/10.1016/j.asr.2018.11.014, 2018.

Yao, Y., Liu L., Kong J., and Zhai, C.: Global Ionospheric Modeling Based on Multi-GNSS, Satellite Altimetry and Formosat-3/COSMIC Data, GPS Solut., 22, 104, https://doi.org/10.1007/s10291-018-0770-6, 2018.

Zakharenkova, I. E., Cherniak, Iu. V., Krankowski, A., and Shagimuratov, I. I.: Vertical TEC representation by IRI 2012 and IRI Plas models for European mid latitudes, Adv. Space Res, 55, 2070-2076, https://doi.org/10.1016/j.asr.2014.07.027, 2015.

Zhang, S., Foster, J. C., Coster, A. J., and Erickson, P. J.: East-West Coast differences in total electron content over the continental US. Geophys, Res. Lett., 38, L19101, https://doi.org/10.1029/2011GL049116, 2011.

Zhang, S., Chen, Z., Coster, A. J., Erickson, P. J., and Foster, J. C.: Ionospheric symmetry caused by geomagnetic declination over North America, Geophys. Res. Lett., 40, 5350-5354, https://doi.org/10.1002/2013GL057933, 2013.

Zhao, B., Wan, W., Liu, L., Yue, X., and Venkatraman, S.: Statistical characteristics of the total ion density in the topside ionosphere during the period 1996-2004 using empirical orthogonal function (EOF) analysis, Ann. Geophys., 23, 3615-3631, https://doi.org/10.5194/angeo-23-3615-2005, 2005.

Uwamahoro, J. and Habarulema, J. B.: Modelling total electron content during geomagnetic storm conditions using empirical orthogonal functions and neural networks, J. Geophys. Res. Space Physics., 120, 11,000-11,012, https://doi.org/10.1002/2015JA021961, 2015.

Wan, W., Ding, F., Ren, Z., Zhang, M., Liu, L., and Ning, B.: Modeling the global ionospheric total electron content with empirical orthogonal function analysis, Sci. China Tech. Sci., 55, 1161-1168, https://doi.org/10.1007/s11431-012-4823-8, 2012.